MSc Thesis report

Modelling calving of Antarctic ice shelves with Machine Learning

Francesco Moncada

Utrecht University

MSc thesis internship carried out at the Institut des Géosciences de l'Environnement, Université Grenoble Alpes.

05.01.2023

Supervisors:
Dr. Romain Millan
Dr. Jordi Bolibar
Dr. Peter Kuipers Munneke

Abstract

Accounting for the evolution of Antarctic ice shelves is crucial for predicting future sea-level rise. While their role in buttressing tributary glaciers is recognized, modeling these complex systems has not yet achieved the accuracy of many other components of the Earth and ice sheet systems. Modeling accurately ice shelf evolution faces challenges, particularly with ice calving, responsible for almost half of Antarctica's ice shelf mass losses. The existing approaches have seen a significant increase in their complexity, making their generalization challenging on a large scale, and they remain confined to specific cases. Even more significant limitations arise from our limited understanding of highly nonlinear processes such as ice shelf damage, which is inherently connected to calving but is not represented in existing methods. The massive influx of satellite imagery data, measuring physical parameters of ice shelves, however, opens the door to new data-driven approaches. These new methods which have largely been underused to model calving, are based on the use of machine learning, and allows capturing highly nonlinear processes by jointly utilizing multi-source observational data. In this study, we employed a data-driven approach to predict calving for Antarctic ice shelves using machine learning models. We chose to predict ice shelf calving using crucial parameters that can influence the rate of iceberg removal from ice shelf faces. These parameters are summarized as: ice shelf basal melting, ice shelf thickness, ice shelf velocity, and sea ice concentration. These were measured from space using multiple sensor remote sensing data, which were analyzed and standardized. The standardization of the dataset includes resampling all variables to the same spatial and temporal resolution, and the the design of an interpolation scheme to assemble a comprehensive dataset. From this work, we assembled two distinct datasets: a data cube incorporating spatial and temporal evolution, and a tabular one integrating spatial information ice shelf-wise near the ice front. We then used the tabular dataset to train a Random Forest model, implementing two cross-validation strategies. The first ensured balanced data representation across folds, respecting spatiotemporal structures in the dataset, while the second involved a random split of the data. Unfortunately, the model failed to accurately predict ice calving in both cases. We attribute this failure to substantial information loss resulting from the spatial information reduction during the construction of the tabular dataset. Although allowing for simpler data representation, the failure of this simple approach suggests the exploration of data driven methods that are able to capture the strong spatial dimension of the dataset (e.g. how changes in the grounding line or shear margins will affect ice shelf calving). For the next steps of this project, which is to be continued beyond the scope of this MSc thesis, we propose using the data cube to feed more complex machine learning methods, such as a Convolutional Neural Network (CNN), which are specifically designed to account for spatial information.

Contents

1 Introduction

This section offers an overview of crucial elements essential for comprehending and predicting sea level rise, focusing on the impact of cryospheric components. Subsection 1.1 emphasizes the significance of glaciers and ice sheets in climate regulation and their pivotal role in global sea level rise projections. In 1.2, the focus shifts to ice shelves, exploring their role in buttressing glaciers and the dynamic interplay influencing Antarctica's mass balance. Additionally, 1.3 delves into the complexity of Antarctic ice shelf mass balance, highlighting the importance of basal melting and ice calving. Subsection 1.4 reviews existing laws for modeling ice shelf calving, while 1.5 outlines the scientific and technical objectives guiding this study.

1.1 Cryospheric components role in Sea Level Rise

Glaciers and ice sheets, often referred to as the Earth's cryospheric components, play a significant role in the context of our planet's climate system. They function as critical climate regulators, acting as vast stores of freshwater that influence regional and global climates. Moreover, they are central to the global averaged sea level rise (SLR) projections, a phenomenon that poses profound challenges for coastal communities and ecosystems. For those reasons, the understanding and the predictions of glaciers and ice sheets evolution is crucial, not just from a scientific prospect but also from a social one. According to the latest Intergovernmental Panel on Climate Change (IPCC) release, the observed SLR between 1993-2010 has been of $3.2 \pm 0.4 \frac{\text{mm}}{\text{yr}}$, with the largest contribution coming from thermal expansion, which accounts for $1.1 \pm 0.3 \ \frac{\text{mm}}{\text{yr}}$. Then, among the other sources $0.76 \pm 0.37 \ \frac{\text{mm}}{\text{yr}}$ are coming from glaciers (excluding Antarctic and Greenland ones), $0.43 \pm 0.11 \frac{\text{mm}}{\text{yr}}$ overall from Greenland and $0.27 \pm 0.11 \frac{\text{mm}}{\text{yr}}$ from Antarctica. The future contribution to sea level rise (SLR) by each source for the year 2100 depends on the scenario adopted in the simulations. Nevertheless, all scenarios agree that the contribution from the Antarctic region, recognized as the largest reservoir of freshwater on Earth, will be significant and characterized by substantial uncertainty.

1.2 Ice Shelves role in buttressing glaciers

Ice shelves are floating platforms of ice that extend to the sea, an extension of land ice which is formed when glaciers or ice sheet flow down into the ocean surface, driven by gravity. Because of their double exposure to air above and water below they are more sensitive to rising temperature than glaciers, and represent therefore a good indicator of environmental change; in the Antarctic region they cover 75 % of the coast, for a total of 1561 square kilometers. Ice shelves play a very important role in buttressing their tributary glaciers, since they regulate the flow of the ice which is directed to the sea: if a collapse of a ice shelf happens the ice discharged into the sea generally experiences an acceleration, and the glacier retreats. This phenomenon was anticipated by theoretical and pioneer studies such as the one from Weertman [1], and in the recent years was validated by observation based studies such as the analysis on Larsen B ice shelf collapse by Rignot [2], and also by modeling ones such as the ABUMIP one [3], where the sensitivity of 15 glaciers was analysed after the (modeled) abrupt removal of the ice shelf: in both case the ice discharge from the ice shelf into the ocean increased significantly. As reminded in the last IPCC, the incapability of the current models to reproduce the ice sheet dynamics of the Antarctic Ice sheet is one of the main reasons which prevents to quantify SLR contribution from Antarctic glaciers, which remains with a high uncertainty and is still far from reaching the same level of development that exists for modeling many other components of the Earth system.

1.3 Antarctic Ice Shelf Mass Balance

The Antarctic mass balance is predominantly governed by the dynamic interplay of ice accumulation and ablation processes. Accumulation involves the net deposition of snowfall, gradually compacting into glacial ice over a specified time frame. Ablation encompasses ice loss through basal melting, ice calving, and surface melting. Basal melting and ice calving constitute the primary loss mechanisms, defined as the quantity of ice melted at the basal part of the ice shelf and the physical process by which ice chunks are discharged into the sea from the terminal part of ice

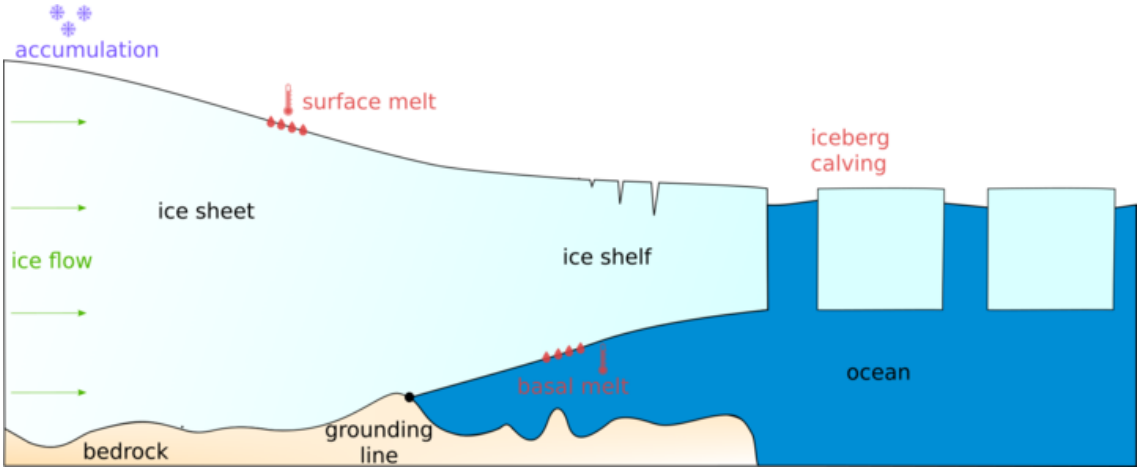

Figure 1: Scheme summarising the physical processes happening in ice shelves

shelves, respectively. Surface melting represents mass loss due to melting at the ice shelf surface from warmer air temperatures.

The first estimation of Antarctic ice shelf mass balance comprehensively covering all Antarctic ice shelves, was conducted by Rignot in 2013 [4], who compared flux divergence, surface accumulation, and ice thinning between 2008-2009. The analysis revealed that the main contributors to mass loss are basal melting and ice calving, accounting for $1325 \pm 235 \frac{Gt}{yr}$ and $1089 \pm 139 \frac{Gt}{yr}$, respectively, while surface melting is negligible compared to the former two.

Basal melting and ice calving are recognized as primary factors contributing to the weakening of Antarctic ice shelves. Basal melting and iceberg calving are crucial processes: by thinning the ice shelves, or changing its surface area, these two processes are reducing the buttressing effect of ice shelves, leading to accelerated glacier flow [5], and greater ice discharge into the ocean [2]. While surface melting's impact on the Antarctic mass balance is generally negligible, it has been suggested to play a role in ice shelf collapse, particularly in the Antarctic Peninsula [6]. Extreme climatic event, such as atmospheric rivers, dramatically enhances surface melt-ponding on top of ice shelves, which has the potential the modify the thermal regime of the ice, propagate cracks and trigger complete disintegration, such as it has been observed for Larsen A-B.

The consequences of ice shelf weakening include collapse, as discussed earlier [2] [3], resulting in

increased ice discharge into the sea and large calving events. Notably, Pine Island Glacier exhibited accelerated ice flow velocity after three significant ice calving events between 2017 and 2020. A model study by Sun et al [7] aimed to understand the drivers behind this acceleration. According to their results, while calving contributes to velocity changes, it alone does not explain the entire acceleration. Ice shelf damage, particularly in marginal areas providing lateral support, also plays a significant role. The increase in ice flow velocity generates stress, leading to ice shelf damage and facilitating further calving events. They suggest those processes to be linked, since increased calving would accelerate further ice flow velocity and therefore also the lateral ice shelf damage, resulting in a positive feedback. An accurate estimation of ice calving is therefore necessary to make reliable predictions of the future Antarctic mass balance, and ultimately of the SLR.

1.4 Existing ice shelf calving laws

Modeling ice shelf calving is therefore essential to predict the future changes in ice shelf mass balance, and contribution of Antarctica to sea level rise. At the moment, a reliable predictive mathematical formula for calving does not yet exist, and most of the attempts to model this phenomenon have been focused on Greenland, for a limited number of tidewater glaciers [8]. In a recent study, the Ice-sheet and Sea-level System Model (ISSM) was employed for the first time to test and evaluate four different existing laws of calving on ten Antarctic ice shelves [9]. Each of these calving laws was parameterized under the assumption that the current position of the ice front is in steady state. The study aimed to find for each ice shelf the set of parameters that best achieves this position over a simulation period of 200 years. The calving laws that were tested can be summarized as follow:

- Crevasse-depth calving law [10]: this law is based on the presence of surface crevasses, and predict calving events to happen based on the ability of one crevasse to separate a block of ice from the rest of the glacier. The paper from [11] modified the calving law from Benn et al, in order to better apply it to large floating ice shelves. In that modified version, the authors accounted for changes in speeds between the grounding line and the middle of the

ice shelf, along with the propagation of basal crevasses.

- Von Mises stress calving law [11]: according to this law calving happens as a consequence of loss in resistive stress, leading the ice shelf to ice flow acceleration and thinning. This law is therefore mainly dependant on tensile stresses, frontal speed and a simple minimum thickness threshold for calving.

- Eigencalving law [12]: in this law the calving rate is predicted according to the first-order kinematic eigenvector, which accounts for the main direction through which ice flows. This calving law is therefore mainly dependant on the accross and along flow strain rate on the ice shelf.

- Minimum Thickness law: this law is a position law, simply stating that calving occurs when the condition $h < h_{min}$ is verified, where h is thickness and h_{min} is some minimum ice thickness threshold settable by a model tuning.

The calving laws which performed better in reproducing the current front positions are the Von Mises and the eigencalving ones, another indication of the primary importance of ice flow velocity and ice stress in predicting calving events. These calving laws remains however limited for example because of their steady state assumption and the fact that they do not include any damage criteria, which plays a central role in calving [7]. The recent availability of massive amounts of satellite derived products (ice front position, ice velocity, thickness...), there is the potential to reach another level of understand of ice shelf calving, and the processes that are driving it.

While most of the studies about modeling ice shelf calving present a classical physically based approach, the full potential of a data driven approach has not been employed in Antarctica. A data driven approach emphasizes the utilization of extensive datasets to empower algorithms in identifying patterns and making predictions, without explicit programming the physical laws. In glaciology, this methodology involves employing machine learning techniques to analyze diverse datasets, such as satellite imagery or climate records. The use of machine learning models has significantly advanced in glaciology and earth sciences in general. Despite the challenges in inter-

preting these models, often referred to as "black boxes," their power lies in the ability to overcome limiting assumptions from parameterizations, while capturing highly non-linear processes [13]. Furthermore, the development of hybrid approaches, allowing the incorporation of physical information into neural networks ("physics informed neural network"), opens the door to a higher degree of interpretability in these methods [14] [15] [16]. Consequently, the development and the democratization of these approaches, combined with the recent availability of large-scale datasets from satellite remote sensing, open new possibilities to face the comprehension of ice calving.

1.5 Objectives of the internship

The scientific objective of this internship is to model iceberg calving at the front of ice shelves in Antarctica using machine learning and investigating its spatio-temporal variability, leveraging large-scale state-of-the-art remote sensing datasets. The first goal involves standardizing extensive remote sensing datasets for predicting iceberg calving. Subsequently, we will assess the performance of two different machine learning approaches. The initial step employs a standard supervised machine learning method, utilizing tabular observations of the ice shelves as input. In the second step, we will evaluate a more advanced approach based on a convolutional neural network (CNN) [17], a model well-suited for simulating data with strong spatial dependencies, such as satellite-based observations. The technical objective of the internship can be described as follow:

- **Assembling the training dataset: standardizing complex and multi-sources observations**

  The initial step involves compiling two standardized, multi-variable datasets incorporating glaciological variables from diverse sources. These datasets encompass the following variables : ice velocity, ice calving, sea ice concentration, ice thickness, and basal melting, derived from various satellite platforms (altimetry, radar, optical sensors, passive microwave instruments) and model outputs. The first dataset, structured cubically, will feed the CNN. For each variable, it consists of 2D layers containing spatial information, with the temporal axis

represented vertically. The second dataset, with a tabular shape, will feed the standard supervised machine learning model. For each variable, it comprises a time series, where each point is derived from the 2D layer of the cubic dataset using different extraction strategies based on the variable. Both datasets will be validated by comparing the results with existing scientific literature.

- **Building the Machine Learning Architecture**
  - **Modelling calving flux on a ice shelf wise base**

    The first standard supervised machine learning model which will be implemented is the Random Forest algorithm [18]. As stated, its input will be the tabular dataset, and it will be programmed to predict the integrated ice calving for each ice shelf. The choice of this algorithm is due to its simplicity and ability to provide valuable physical insights into the underlying processes.

  - **Modelling calving front position with a CNN**

    The subsequent goal would be to implement a CNN, which will take as input the data cube to make spatialised prediction of the ice shelf calving front position. The CNN's ability to recognize complex spatial patterns across different regions of the ice shelf, makes it well-suited for predicting ice calving front positions. Its strength lies in capturing intricate spatial dependencies essential for understanding the dynamics of calving processes.

2 Data and Methods

In this section are described the datasets, the way they were treated and the structure of the model. In 2.1 we describe the datasets in terms of resolution and measurement techniques, and in 2.2 the main problems related to their format and inter-compatibility. In 2.3 we describe the re-scaling procedures adopted to standardize the datasets, and in 2.4 how data gaps were filled with different techniques. In 2.5 we introduce the procedures adopted to derive the time series used to

feed the Random Forest model, and finally 2.6 describes the model itself and of its settings.

2.1 Dataset Overview

2.1.1 Ice Thickness

The ice thickness dataset we used in our work is described in the paper by Paulo et al [19] (from now on Paulo). This dataset merged thickness observation obtained by four European Space Agency (ESA) satellite radar altimetry missions, spanning various time periods and technological specifications, in order to construct a 26 years (1992-2017) dataset of ice shelves thickness, with a 3km grid resolution every 3 months. The mission datasets encompass measurements obtained from a series of satellites: ERS-1 (1991-1996), ERS-2 (1995-2003), Envisat (2002-2010), and CryoSat-2 (2010-2017). The initial three satellites utilized a pulsed-limited altimeter system featuring a spatial frequency of approximately 370m. In contrast, CryoSat-2 employed a dual-antenna Doppler/delay altimeter that operates in synthetic aperture radar interferometric mode (SarIn) with distinct along and across track footprints of 300m and 3000m, respectively. A pulsed-limited altimeter is a radar system that measures the time it takes for a transmitted pulse to travel to the target and back, providing information about the surface topography. SarIn is another radar technique that enhances spatial resolution by combining multiple radar observations, offering a more detailed and comprehensive topography view. Surface elevation from ERS data is obtained by using differential SAR interferometry method, which provides the difference in phase between two acquisition of the ERS satellite during the TanDEM mode mission. The accuracy of the measurements is strongly affected by the slope of the surface, and ranges between 10cm to 100m. In this dataset the Ice shelf boundary definition is derived from a combination of Landsat imagery and ICESat data [20], updated with more recent measurements from MEaSUREs v2 boundaries [21], manually edited for significant calving events from satellite imagery.

2.1.2 Ice Velocity

The dataset used to analyse the ice flow velocity is the MEaSUREs InSAR-Based Antarctica Ice Velocity Map Version 2, released by Nasa [21], which provides both x and y velocity components.

The 450m spatial resolution grid extends over the whole antarctic region in stereographic polar projection, and has a yearly temporal resolution. The dataset was made by combining the measurements of 3 different sensors, one working in visible part of spectrum (Landsat-8), and two others in synthetic aperture radars working at C-band, 5.405 GHz or 56 mm wavelength (Sentinel-1a/b and RADARSAT-2). Ice velocity is calculated by performing feature (tracking crevasses) or speckle tracking (tracking speckle on SAR data) on optical (or radar) images of the same area, taken at a different time. Those estimations rely on cross-correlation analysis, a technique which involves comparing patterns in radar/optical images at different times and identifying peaks in correlation to estimate ice movement. Recent progress in processing chains allowed to automatize the processing, the calibration and the mosaicking of the different sources of satellites, in order to create a product which is spatially and temporally coherent and as complete as possible. Although this dataset represents the state of the art for ice velocity in Antarctica, there still remain many spatial deficiencies and lapses. In particular for certain years, the dataset spatial coverage of the Antarctic region is very limited, and vast areas remain without any ice flow velocity information. In order to compensate these deficiencies, two other datasets were used to integrate it.

The first one was released by Mouginot et al in 2019 [22], in which they managed to obtain a $20\frac{cm}{yr}$ ice flow velocity resolution map of Antarctic ice flow velocity. They obtained it by combining interferometric phase data from a series of SAR satellites acquired over 25 years, from 1992 to 2017. The SAR satellites are RADARSAT-1 and RADARSAT-2 from the Canadian Space Agency, ERS-1, ERS-2, and the Envisat ASAR from the European Space Agency, and the Japan Aerospace Exploration Agency. The map is obtained by mosaicking and averaging the data over the 25 years, and therefore does not present time evolution.

The second dataset integrated into our analysis is constrained to the Amundsen Bay environment [23]. This dataset, part of the NASA Making Earth System Data Records for Use in Research Environments (MEaSUREs) Program, comprises high-resolution digital mosaics capturing ice motion in the Amundsen Sea Embayment and West Antarctica, including the Pine Island, Thwaites, Haynes, Pope, Smith, and Kohler glaciers. The mosaics were compiled from InSAR data collected

during 1996, 2000, 2002, and 2006-2012 by various satellites from European and Canadian space agencies, as well as Japanese and German aerospace agencies. The precision of this dataset varies by region, ranging from a minimum of $6\frac{m}{yr}$ to a maximum of 20 $\frac{m}{yr}$.

2.1.3 Basal Melting

Basal melting rates are obtained by solving the equation of mass conservation over ice shelves as follow:

$$\dot{b}(t) = \frac{\partial H}{\partial t} + \nabla \cdot (Hu) - \dot{a},$$

for $\dot{b}$, the basal melt rate. $\frac{\partial H}{\partial t}$ is ice thickness time derivative, $\nabla \cdot (Hu)$ is ice-flux divergence, u is velocity and $\dot{a}$ is surface accumulation rate (SMB). The dataset we used originates from the combination of satellite radar altimetry, ice flow velocities, surface mass balance and firn models [19]. Changes in ice thickness are estimated from radar altimetry, that estimates the ice shelf surface elevation, and converts it into ice thickness using the hydrostatic equilibrium assumption. The satellite that were used inside [19] are the ESA's radar sensors ERS-1 (1991–1996), ERS-2 (1995–2003), Envisat (2002–2010), and CryoSat-2 (2010–2017). The surface mass balance $\dot{a}$ was obtained by calibrating observation and modelled snow density profile, while velocity u was obtained by merging different products, such as the InSAR-based velocity [24] and, for ice shelves where ice velocity does not changes significantly, the optical-based time-aggregated velocity of Gardner [25]. For regions where the ice flow velocity experienced relevant changes, such as the Amundsen sea sector, the authors integrated datas from NASA MEaSUREs project [23].
The original data are presented as netCDF files with a bi-yearly mapping of basal melting rates, at grid cell-size of 2-km. The ice shelves fronts are dynamically moving while the grounding lines of the ice shelves are kept fixed. This is a limitation of the dataset that may have important consequences on the evolution of melting rates through time, since the rates of meltings are expected to be the highest in the grounding line region. Hence, if the grounding line has migrated tens of kilometers inland, as it was observed in the Amundsen Sea Embayment, the highest melting values are being automatically discarded. However, since the dataset from [19] is the only one available as such a resolution and temporal coverage, we decided to keep using it. The first pre-

processing step was to calculate yearly averages of the spatially distributed basal melting rates in order to be on the same temporal time scales as the calving rate dataset [26]. The second processing step was to assemble a basal melting dataset in the form of tabular data, in order to feed our first machine learning approach. To do this, we decided to calculate integrated values of basal melting rates for each ice shelves. For each year, we first corrected the melt rates values for the pixel distorsion due to polar stereographic projections [19], and summed all of the basal melting pixels for each of the ice shelves, and finally converted the values from meters of per years of melt to gigatons per year of melt.

2.1.4 Sea Ice concentration

The dataset employed for studying sea ice concentration, defined as the fraction of the ocean covered by sea ice, is the NOAA/NSIDC Climate Data Record of Passive Microwave Sea Ice Concentration Version 4 [27]. These data products are derived from observations made by the Scanning Multichannel Microwave Radiometer (SMMR) instrument aboard the Nimbus-7 satellite, as well as the Special Sensor Microwave/Imager (SSM/I) and Special Sensor Microwave Imager/Sounder (SSMIS) instruments carried by the Defense Meteorological Satellite Program's (DMSP) satellites. Sea ice concentration is estimated through satellite measurements of brightness temperature, combining the results of two GSFC-developed algorithms: the NASA Team algorithm [28] and the Bootstrap algorithm [29]. The data cover the entire sea of the Southern Hemisphere with a spatial resolution of a 25 km grid in polar stereographic projection, making it much coarser than the other datasets; its time resolution is monthly.

2.1.5 Ice Calving

For the study of ice calving, the target variable of this research, we utilized the dataset produced by Greene et al [26] (from now on, Greene et al), which we integrated with the BedMachine mask [30]. The BedMachine mask contains the state-of-the-art bed topography/bathymetry map of Antarctica with a spatial grid of 500m, derived using a mass conservation algorithm on airborne radar measurements. The Greene et al dataset presents both the ice shelves' evolving coastlines,

with a spatial grid resolution of 240m and a temporal resolution of one year, and the yearly cumulative ice loss due to calving for each ice shelf. The cumulative ice loss is defined as the sum of both the mass changes attributed to annual fluctuations in the front position and the steady-state calving rate. The coastlines were calculated by first manually mapping the fronts of ice shelves, combining three different datasets, namely RAMP [31], MOA [32], and MODIS [32]. On the other hand, the authors calculated the steady-state calving rate of the glacier by deriving the ice flux at the most retreated front position, combining both velocity and thickness observations, namely ITSLIVE [33] and MEaSUREs InSAR-Based Antarctica Ice Velocity Map version 2 [21] for velocity, and Bed Machine v2 for thickness [34].

To generate a dataset for predicting the calving front position, we extracted the coastline positions from the Greene et al dataset on a yearly basis. The format of the coastlines consists of datapoints regularly spaced by 240 meters along Antarctica's margins, which we converted into lines, polygon shapefiles, and finally into raster format using tools from the Quantum GIS software. The coastlines of Antarctica are then combined with the BedMachine mask to delineate floating ice, grounded ice, rock outcrops, and open ocean using Python. The ice shelf area is modulated by the Greene et al coastline dataset, with grounding line positions derived from Quadruple Differential SAR Interferometry [35]. Similar to the basal melting product, one limitation of our approach is in the Amundsen Sea Embayment, where our method does not account for potential grounding line migration, which has reached several tens of kilometers in this area [36].

2.2 Dataset analysis

Although all the datasets we adopted represent the state of the art for Antarctic remote sensing measurements, we encountered several challenges during our analysis related to their completeness and intercompatibility. The main issues are summarized here:

- Different resolution:

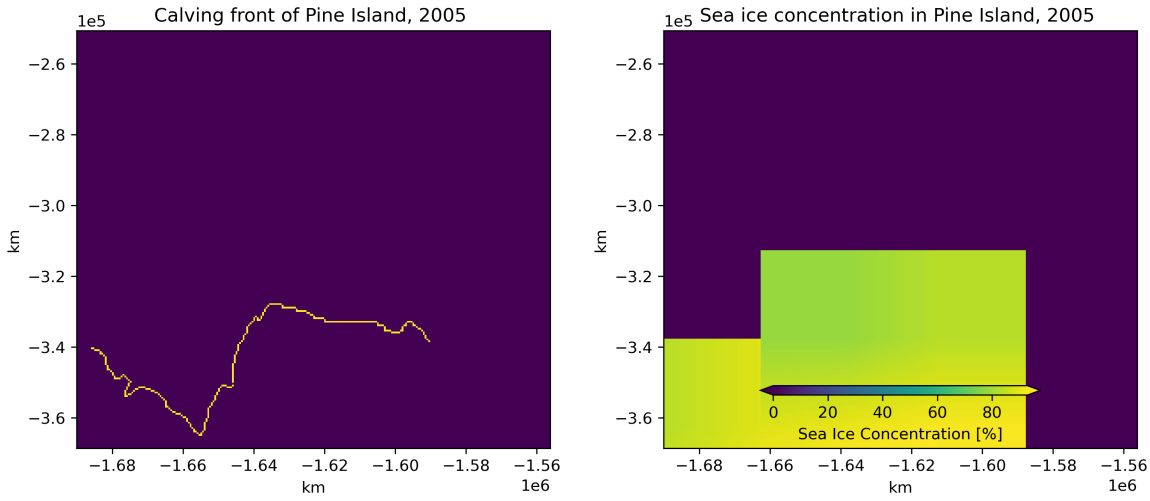

Figure 2: The datasets exhibit significant variability in spatial resolution. Here we depict two extremes: the calving front (left) and the sea ice concentration (right), with resolutions of 240m and 25 km, respectively.

Datasets exhibit significant variability in terms of temporal and spatial resolution, necessitating uniform rescaling for comparison and processing. Spatial resolution ranges from the 240m grid of the ice calving dataset to the 25 km resolution of the sea ice concentration dataset, as illustrated in Figure 2. Temporally, they all have a yearly frequency, except for the sea ice concentration dataset, which is updated monthly.

- Different time extension:

  The time range covered by each dataset varies. For our final dataset, we selected a time range that is common to all datasets, spanning from 2005 to 2017.

- Data coverage:

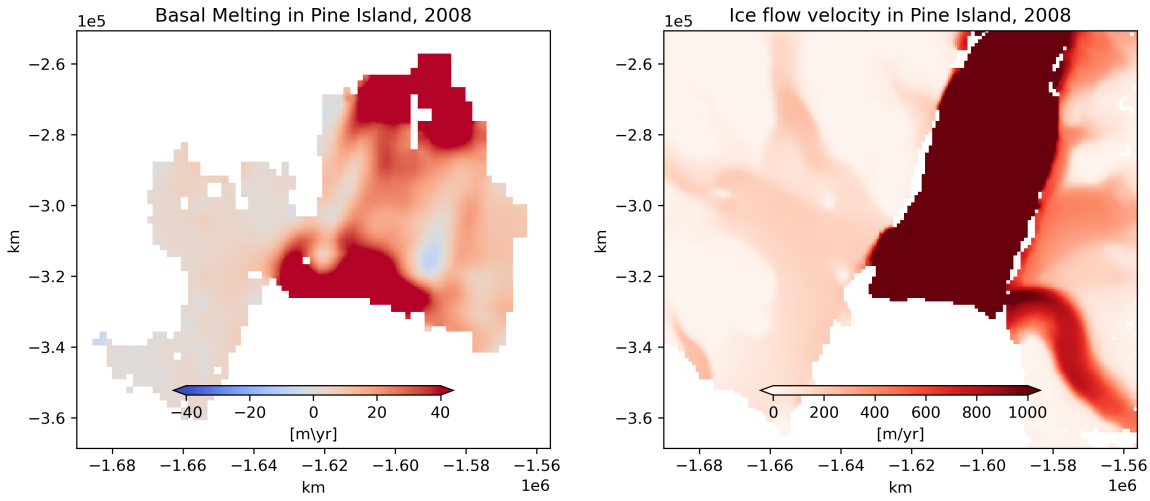

Figure 3: Example of two different data coverage for basal melting and ice velocity.

The regions covered by each dataset vary. For instance, basal melting and ice thickness data are available only within the border of the ice shelf, as depicted in the left panel of Figure 3. In contrast, ice velocity data extend also to the surrounding grounded ice, as shown in the right panel of Figure 3. From the perspective of the CNN model, this poses a limitation for the ice thickness dataset due to the absence of boundary conditions.

- Missing Data:

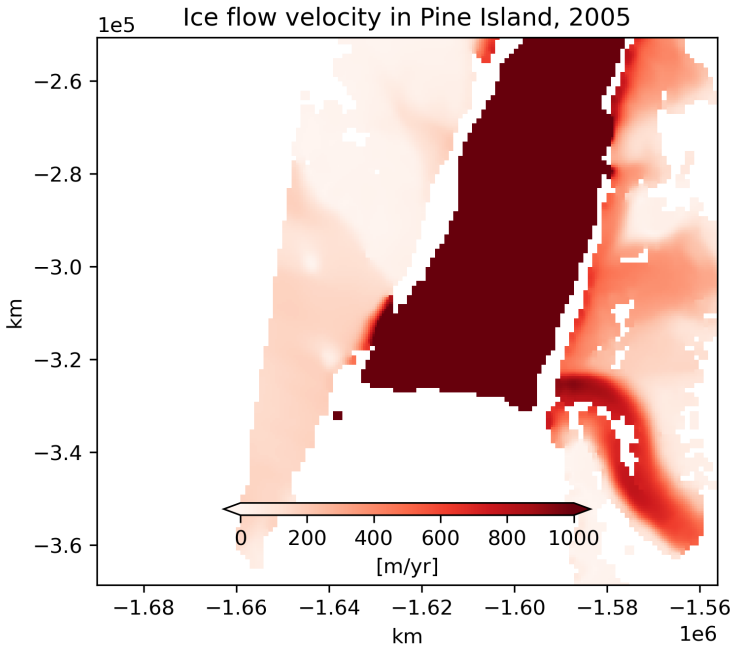

Figure 4: The ice flow velocity dataset presents many missing data, here is reported as an example the data coverage for the ice shelf Pine Island in 2005.

While most of the datasets are complete in terms of data, the ice flow velocity dataset exhibits numerous gaps and lapses, as illustrated in Figure 4, especially for certain years. In the year 2011, the majority of the ice shelves have a spatial data coverage of less than 25% of the region, making interpretation and treatment of these data particularly challenging.

- Ice shelves geometry:

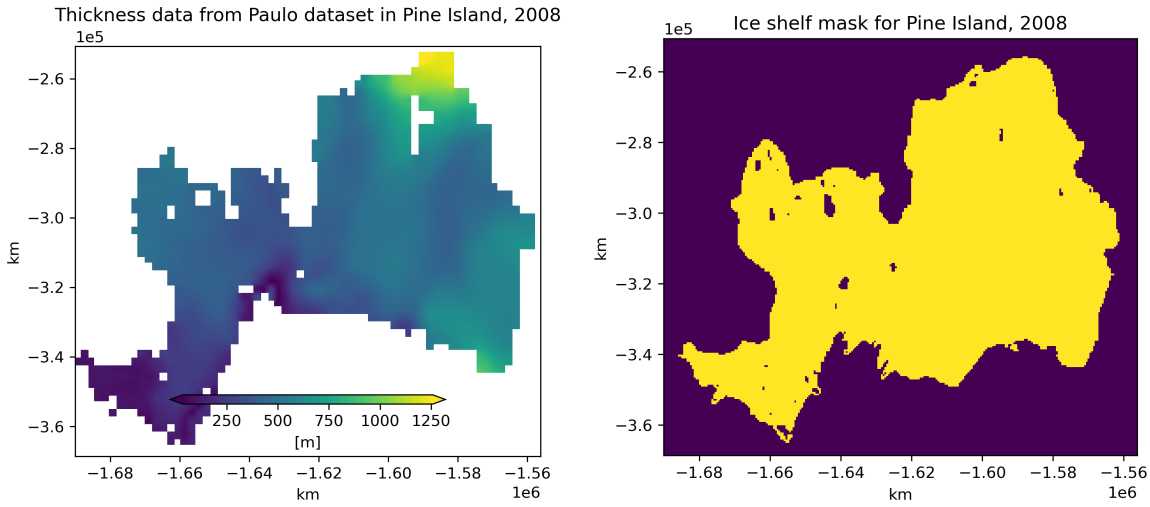

Figure 5: The shape of the ice shelf differs between datasets. In this example, the left side shows the ice thickness of the floating ice according to the Paulo et al dataset, while the right side displays the floating ice shelf mask derived from the Green et al dataset. As observed, the Greene et al dataset indicates that the ice calving front advanced between 2005 and 2008, whereas Paulo's dataset does not report this event.

The shapes of the areas containing floating ice are not consistent across different datasets. In the case of ice calving, the ice shelf front position evolves every year. However, in the ice thickness and basal melting datasets it remains constant for different years before changing, while In the sea ice concentration one remains constant throughout the entire period we considered. We assumed that the dataset derived by the Greene et al dataset contains the 'true' calving position. This assumption introduces a problem in cases where discrepancies emerge, manifesting as mismatches in ice floating shapes between different datasets. This anomaly arises due to ice calving events, leading to the collapse of the front, which was not registered in the Paulo or sea ice concentration datasets. Conversely, there are regions lacking data where, according to the Greene et al dataset, the ice front position has advanced, but this advancement was not registered in the others, as shown in the example in Figure 5. Addressing these discrepancies is crucial for an accurate assessment of ice shelf dynamics and understanding the impact of calving events.

2.3 Dataset rescaling

To facilitate the comparison and processing of datasets, we adopted the resolution of BedMachine v3 as the standard, set at a pixel size of 500 meters in a polar-stereographic projection. This choice is justified by the widespread use of this dataset in the Antarctic modeling community, making it a common standard for data-sharing. For datasets that were upscaled (calving front and ice velocity), we applied average interpolation. Conversely, for datasets that were downscaled (sea-ice concentration, thickness, and basal melting), we used bilinear or cubic interpolation. All operations were performed using the GDAL Python library. Regarding the temporal resolution, we opted for the coarser frequency, which is yearly. Therefore, we calculated yearly averages for basal melting rates and sea ice concentration.

2.4 Dataset interpolation

Since we assumed that the most realistic shape of the ice shelves is derived from the Greene et al dataset, we adapted all the other datasets to have the same regional features. To achieve this, we used the dataset derived from Greene et al to identify regions covered by floating ice, grounded ice, rock outcrops, and open ocean. By comparing these features with other datasets, especially for floating ice, each grid point has two possible outcomes:

- The point is covered by floating ice in the Greene et al derived dataset but not in the others (calving front advance was not registered in the other datasets).
- The point is not covered by floating ice in the Greene et al dataset, but it should be covered according to the other datasets (calving front collapse was not registered in the other datasets).

For the latter case, we simply set the values of the variables outside the ice shelf to zero. However, for the first case, we had to interpolate the values to fill the entire domain. Since each dataset differs significantly from the others, the strategies adopted vary considerably for each dataset and are described in the next subsections.

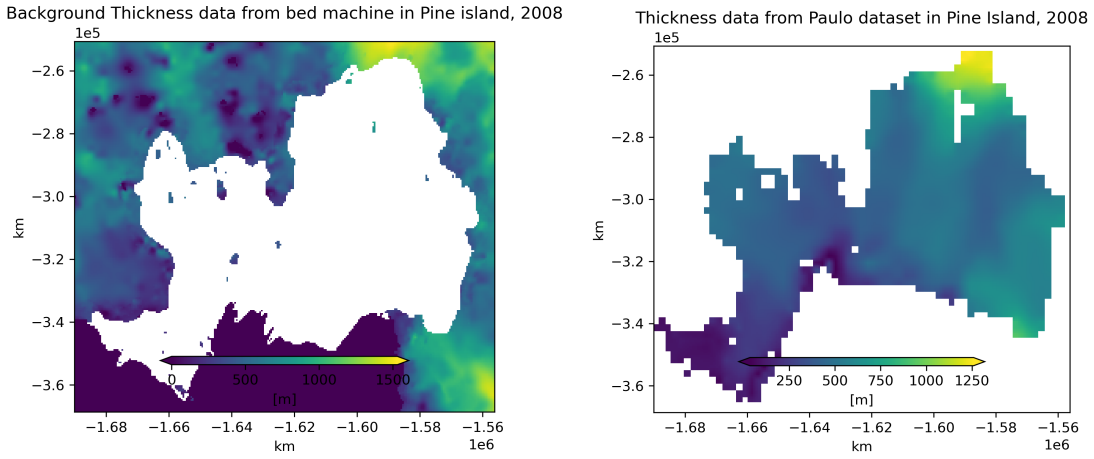

Figure 6: On the left panel, the ice thickness in Pine Island extracted from BedMachine and the floating ice mask (in white), derived from the Greene et al dataset, are shown. On the right panel, the ice thickness from Paulo for the same region in the year 2008 is displayed. Noticeably, the regions for floating ice in Green et al and Paulo datasets do not coincide. While Greene et al and Paulo datasets evolve over time, BedMachine remains constant.

2.4.1 Interpolating Ice Thickness

As previously stated, the ice thickness dataset from Paulo et al includes thickness measurements only for the floating ice of the ice shelf, which does not have the same shape as the Greene et al dataset, as shown in Figure 6. Consequently, the boundary conditions are not defined for ice thickness, potentially leading the CNN to misinterpret the input thickness variable. To address this, we opted to integrate the missing information by extracting thickness data from the BedMachine dataset. BedMachine contains ice thickness information for the entire Antarctic region, although it is time-independent and thus presents the same background for all the years. For each ice shelf, we decided to fill the regions covered by grounded ice, land, and ocean (according to the Greene et al derived dataset) with thickness data obtained from the BedMachine dataset. Simultaneously, we removed all data from the regions that, according to the Greene et al dataset, are covered by floating ice. This process is illustrated in the left panel of Figure 6, where ice thickness data from BedMachine is presented. The floating ice mask, derived from Greene et al for Pine Island in 2008, is emptied of data and highlighted in white.

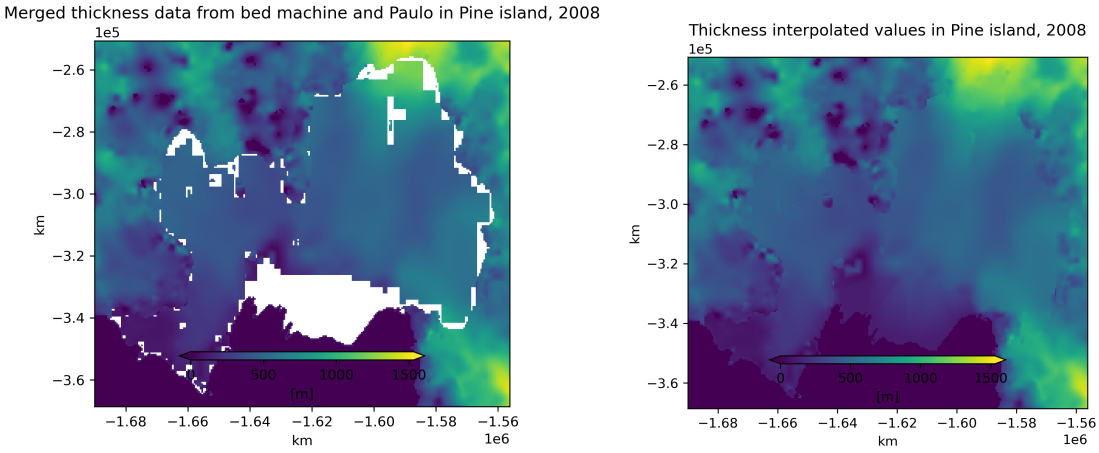

Figure 7: On the left panel is reported the merging of the dataset from bed machine and Paulo datasets, on the right one the image resulting from their interpolation.

Therefore, we filled the regions emptied of data with the ice thickness retrieved by Paulo, visible in the right panel of Figure 6. This operation inevitably leaves some regions without any data, as shown on the left panel of Figure 7. We decided to fill these regions by performing a linear interpolation to guarantee a smooth transition at the interface with grounded ice. For many ice shelves, the region to be interpolated is usually between the calving front line position according to the Paulo dataset and the calving front line position according to Greene et al, which is usually further out to sea. This interpolation step is more challenging since the ice shelf front thickness is not zero but rather ends into a vertical face that can be 100 meters thick. To provide a consistent interpolation, we calculated the average ice thickness in the terminal part by automatically delineating a mask in the vicinity of the ice shelf front. To create this mask defining the floating ice borders, we analyzed from the Greene et al dataset which regions are covered by the sea and which ones are covered by floating ice, extracting two separate masks for them. Finally, we expanded the sea mask by 500 m (one pixel) toward the direction of the floating ice, and created the border mask by intersecting the sea expanded mask with the floating ice one.

To obtain the border value, we expanded the border mask by 5000 m (10 pixels) in the direction of the floating ice shelf, creating a mask that covered the terminal part of the floating ice. We

used this mask to calculate an average thickness value in this region, and filled the original border mask with it. After this process, linear interpolation became possible. Although this method presents the limitation of using the same ice thickness value for the entire ice shelf front, it offers the advantage of not wasting but rather exploiting the local information available in the Paulo et al dataset. The resulting interpolated ice thickness for Pine Island ice shelf in 2008 is visible in the right panel of Figure 7.

2.4.2 Interpolating basal Melt

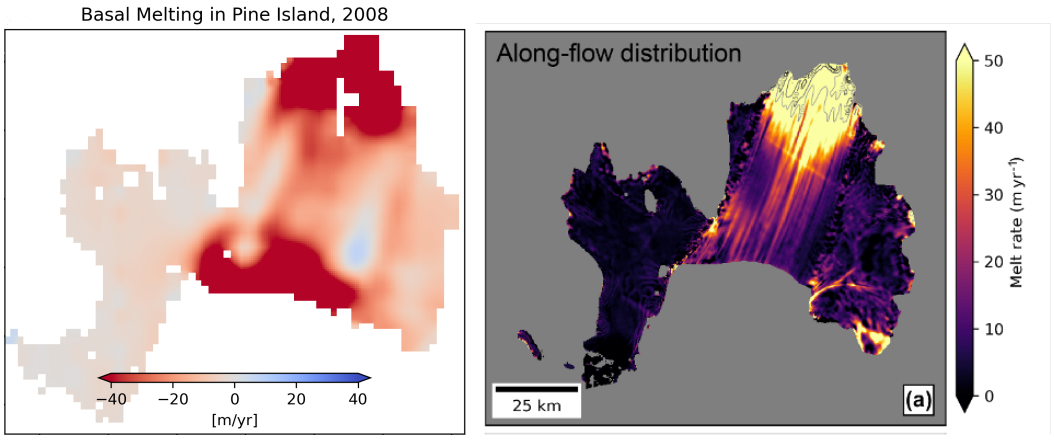

Figure 8: On the left panel is reported basal melting map from Paulo, while on the right one the image retrived from Shean work [37]. As it is possible to notice, the basal melting at the boarder in Paulo is very high, while this is not found in Shean.

Being derived from the Paulo thickness dataset, the basal melting dataset exhibits the same spatial structure. Therefore, also for this dataset a manipulation is necessary to fill the entire domain. Although the background is not as crucial as for the thickness dataset, given that basal melting is zero outside the floating ice shelf region, this dataset presented a different challenge. We observed that for many ice shelves, the regions close to the ice front exhibit very high values, as seen for example in the left panel of Figure 8, where Pine Island basal melting is reported for the year 2008.

We compared the Paulo dataset with another dataset, specifically the work of Shean [37], where

basal melting for Pine Island was estimated using a very high-resolution digital elevation model integrated from SPIRIT imagery along with altimetry data. In the right panel of Figure 8, the basal melting multi-year average from 2008 to 2018 by Shean is reported and it is observable that the frontal values are not as high at the ice front. This aligns with the expected behavior for this type of melting mode, where the melt is highest at the grounding line and decreases toward the ice front, as CDW mixes up with ice freshwater. Such artifacts in the Paulo dataset could be due to the coarse resolution and the rapid fluctuation of the ice front between altimetry measurements, which could result in abnormally high thickness changes.

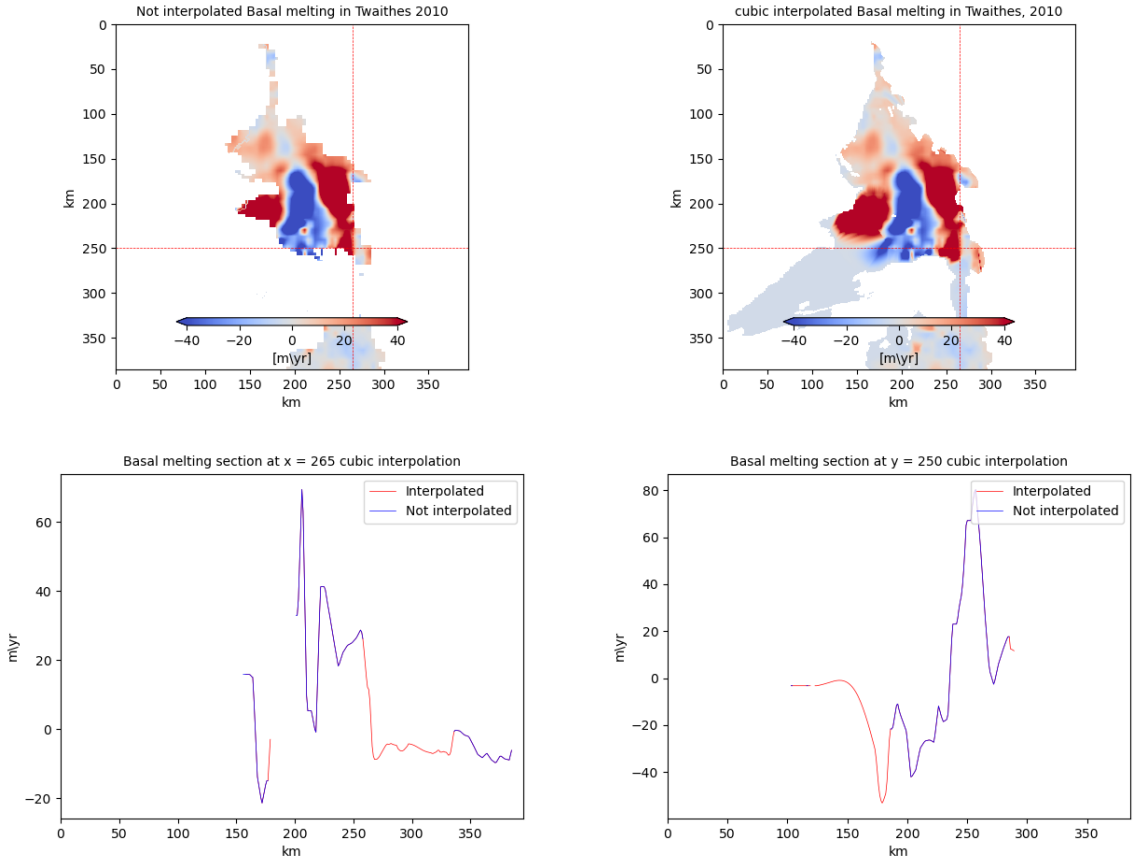

Figure 9: In the upper two panel is possible to see Basal Melting for Twaithes ice shelf in the year 2010, before and after the interpolation. The two lower ones report two sections of basal melting respectively for x = 265 km and y= 250, in the reference sistem of the ice shelf.

To avoid artifacts in interpolating basal melting close to the ice front, we calculated the average of the 30th percentile lowest values in basal melting rates for each ice shelf. The choice of the 30th percentile was made after trial and error tests. This value was then used as a target for the basal melting rates that should be reached at the ice shelf front. This approach aimed to preserve as much data as possible from the original dataset while acknowledging that the dataset is not reliable in the terminal border of the ice shelf. We proceeded to reconstruct basal melting in regions where data was missing, interpolating with scipy library algorithms in Python [38]. Employing a trial and error approach, we tested different types of interpolations and found the cubic one to be the most realistic compared to others (linear and quadratic).

2.4.3 Interpolating Sea ice concentration

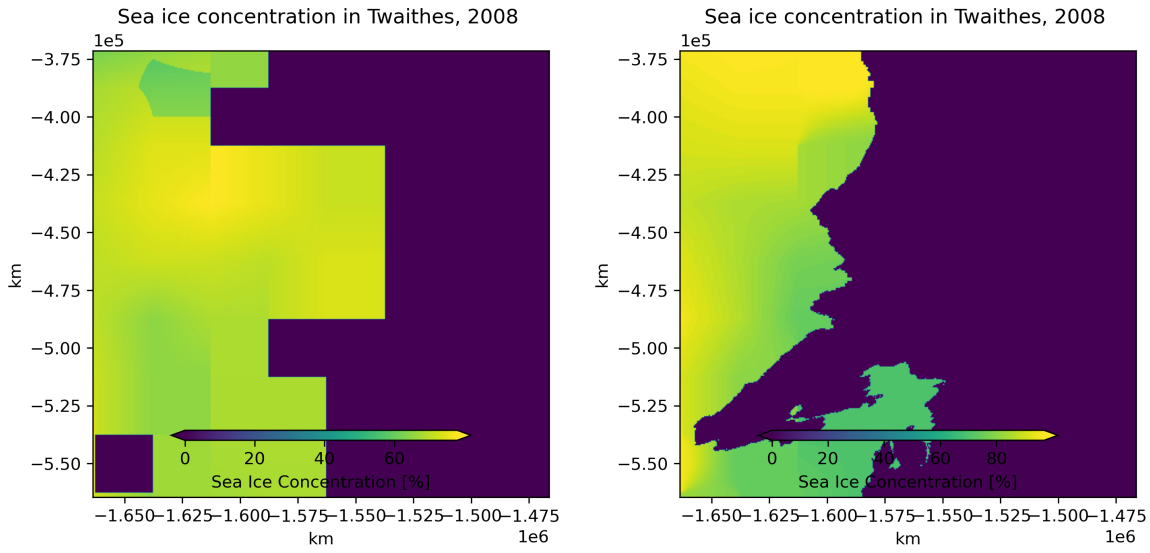

Figure 10: The original sea ice concentration dataset (left) and the interpolated one (right), for Twaithes ice shelf in 2008.

As mentioned earlier, the NOAA/NSIDC dataset containing sea ice concentration has the coarser resolution of 25 km. Despite downscaling its resolution to 500m, the coastlines' shape remains approximate compared to the Greene et al-derived dataset, and numerous oceanic regions exhibit missing data. To address this, we generated a mask for each ice shelf and year, defining the oceanic

areas based on the Greene et al dataset. Subsequently, we applied biharmonic interpolation with an inpaint algorithm to fill the regions with missing data [39]. Biharmonic interpolation is a mathematical technique adept at reconstructing a continuous function from irregularly spaced data points, proving particularly effective in scenarios with missing data. The method involves fitting a biharmonic spline to the available data points, creating a smooth surface that faithfully captures the underlying information.

2.4.4 Interpolating Ice Velocity

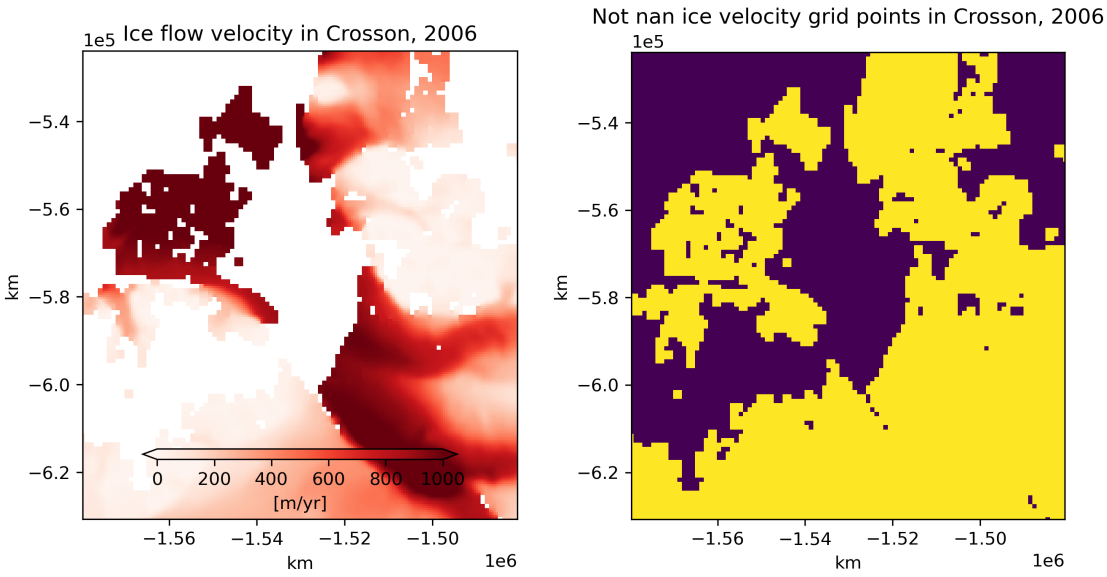

Figure 11: On the left panel is reported the ice velocity for Crosson ice shelf in 2006, on the right one the mask highlighting in yellow the regions where datas are present, for the same image.

The Antarctica Ice Velocity Map Version 2 includes the velocity of both the floating ice and the grounded ice, providing essential boundary conditions for ice shelf flow velocity. However, this dataset poses challenges due to numerous data gaps, especially in the years 2005, 2011, and 2012. During these years, many grid points lack data, resulting in spatial coverage below 25% for the majority of the ice shelves. To maximize the utilization of this dataset and recover as much information as possible, we devised two distinct strategies based on whether the data coverage exceeded or fell below 25%.

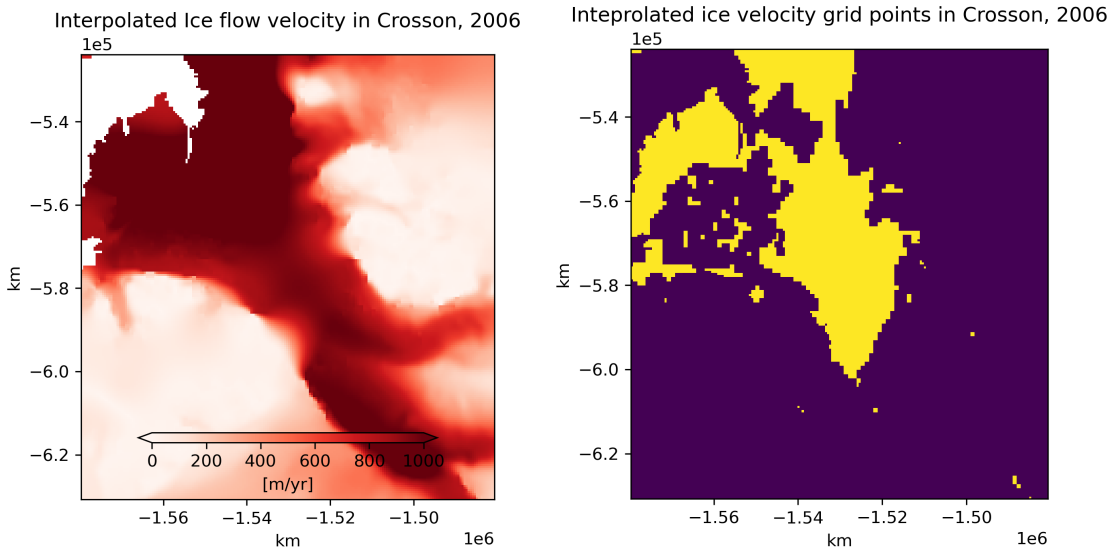

Figure 12: The left panel illustrates the interpolated ice velocity for the Crosson Ice Shelf in 2006, while the right panel displays the mask indicating the grid points that have undergone interpolation.

- If the data coverage exceeds 25%, we employed an inpaint biharmonic algorithm for interpolating the missing areas within the region. The use of this algorithm ensures that the interpolation aligns with the flow lines of the ice velocity, resulting in a more realistic outcome compared to a simple linear interpolation. An example of this technique is illustrated in the left panel of Figure 12, where the ice flow velocity for the Crosson Ice Shelf in the year 2006 has been interpolated. The interpolated pixels are depicted in the right panel.

- In cases where data coverage falls below 25%, a simple interpolation is deemed insufficient for image reconstruction due to a significant amount of missing data. Consequently, we opted to employ a scaling technique using the comprehensive multi-year velocity dataset derived from radar interferometry.

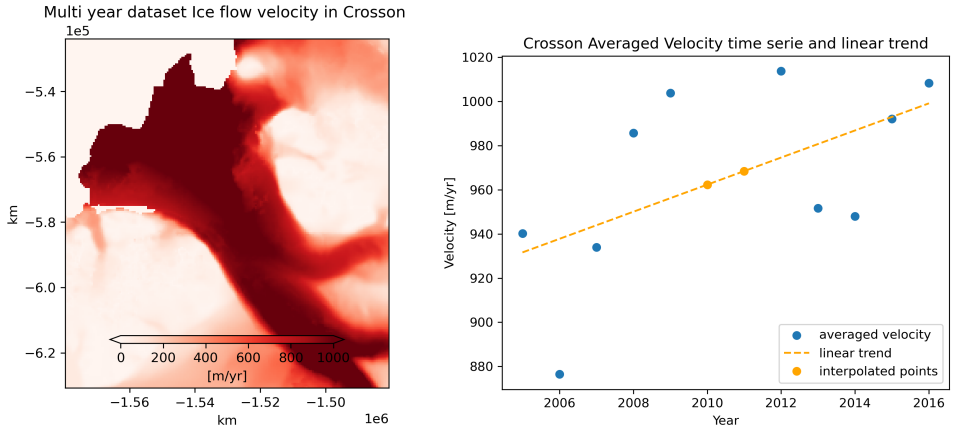

Figure 13: On the left panel, the ice flow velocity of the Crosson Ice Shelf is depicted based on the multi-year dataset. The right panel displays the averaged velocity time series for the Crosson ice shelf, which was utilized for scaling the multi-year dataset. As previously mentioned, the ice flow velocity dataset is significantly compromised for the years 2010 and 2011, prompting us to interpolate the averaged ice velocity points for those years. The interpolated values are then employed to scale the multi-year velocity image.

Multi Year Velocity Dataset Treatment: As mentioned earlier, the multi-year dataset offers a static representation of ice flow velocity for the entire Antarctic region, lacking temporal evolution. To overcome this limitation and account for the temporal aspect of ice flow, we rescaled the dataset for years with substantial damage by considering the time evolution of each ice shelf. This process involved extrapolating a linear trend based on the average velocity of each ice shelf, considering only the years where the coverage exceeded 25%. The extrapolated trend was then employed to estimate the average ice flow velocity for the damaged years.

To create a comprehensive average ice velocity time series for each ice shelf, we determined the average velocity from the multi-year dataset for every ice shelf, treating it as a reference. Subsequently, we calculated the ratio between the values from the average velocity time series and the reference value for each ice shelf, resulting in a time series of ratios. These ratios were employed to rescale the multi-year velocity image for years with less than 25% data coverage.

In Figure 13, the unscaled multi-year ice flow velocity for the Crosson Ice Shelf is presented on

the left panel, while the right panel illustrates the time series derived by averaging the ice flow velocity over the entire region. The orange points indicate the estimated values derived from a linear trend for years where data coverage was below 25%, specifically in 2010 and 2011. These points were instrumental in rescaling the multi-year image for the respective years.

2.5 Extracting the tabular dataset

With the cubic dataset finalized, our next step involved extracting the tabular dataset by generating time series for all variables spatially integrated for each ice shelf. This tabular dataset offers a simpler representation of the data. We employed various approaches during this process:

- Extracting variables from the front:

  For ice thickness and sea ice concentration, time series points were extracted from specific regions near the ice shelf border. Utilizing a technique similar to that employed for ice thickness interpolation, we expanded the ice shelf border mask towards the floating ice for ice thickness and towards the sea for sea ice concentration, obtaining values by averaging the two variables in those regions. While this approach results in the loss of overarching trend information for the entire ice shelf, it provides a more precise understanding of the variable's behavior in regions where ice calving occurs.

- Extracting 80^{th} ice velocity percentile:

  For ice velocity, instead of directly focusing on a specific region of the ice shelf, we decided to concentrate on the grid points where the ice flow velocity is greater than the 80^{th} percentile. This decision was made by analyzing the ice velocity dataset and noting that the regions where ice flows faster also experience the greatest changes in velocity, making them the most interesting regions to study and include in the dataset.

- Extracting basal melting and ice calving from the dataset:

  For basal melting, we utilized the integrated values from the basal melting time series derived by Paulo, while for integrated ice calving, we used the Greene et al dataset, which already contains the integrated values per glacier per year.

2.6 Random Forest model implementation

Predicting dynamic phenomena such as ice calving, influenced by various interacting factors, demands a robust and flexible model capable of capturing non-linear relationships. Among the machine learning tools available, we chose the Random Forest algorithm [18]. The Random Forest algorithm combines the outputs of multiple decision trees to produce a single result. Each decision tree is a hierarchical structure of nodes and leaves that guides predictions by recursively partitioning data based on feature values. In this approach, each internal node represents a split of the dataset, and each leaf node signifies an outcome. Each tree operates independently, constructed through recursive partitioning of the data based on the values of various features. At each branching node, the tree determines the most informative feature for dividing the data by assessing the reduction in a chosen error metric for the target variable, within the resulting subsets. The objective is to identify splits that minimize this error, creating subsets with more consistent values for the target variable. This process continues iteratively until predefined stopping conditions are met, leading to the formation of a hierarchical structure of nodes and leaves that collectively define a decision path. The flexibility of decision trees enables them to capture complex non-linear relationships present in the data. However, a single decision tree is susceptible to overfitting, tailoring itself too closely to the training data and limiting its ability to generalize to unseen instances. Random Forest mitigates this limitation by aggregating the outputs of numerous trees. Each tree is constructed using a random subset of the training data and a random subset of features at each split, introducing differences among the individual trees. The final predictive outcome of the Random Forest model emerges from the combined predictive power of the individual trees, with each tree contributing a unique perspective on the underlying patterns within the data. Furthermore, the interpretability of Random Forest is advantageous for discerning the relative contributions of each variable to the predictive model, providing insights into the key factors influencing ice calving events.

In our study, the target variable to predict is the annual ice loss due to calving events for each ice shelf. The model utilizes basal melting, sea ice concentration, ice velocity, and ice thickness as

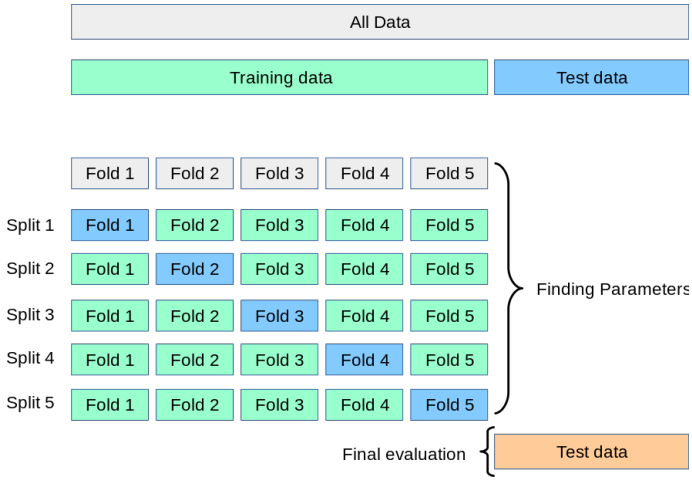

Figure 14: A visualisation scheme for Cross Validation retrived from scikit-learn [40], In the training dataset is possible to see that in each iteration a different fold is used as a test fold (in blue), while the others as training (in green).

input features to make predictions. All data used to train, validate and test our model come from the tabular dataset explained in section 2.5.

2.6.1 Partitioning the dataset

A crucial step in every machine learning pipeline is the implementation of cross-validation, a statistical technique used for hyperparameter selection and to assess the performance and generalizability of a machine learning model. After dividing the dataset into training and test sets, cross-validation partitions the training dataset into multiple subsets called folds. The model is then trained on some of these subsets and evaluated on the remaining data within the training set, contained in the other folds. This process is repeated multiple times, with different folds of the training set used for training and validation in each iteration. Cross-validation helps estimate how well a model will perform on unseen data, providing a more robust evaluation than a single train-test split. It aids in detecting issues like overfitting and ensures that the model's performance is representative across different data subsets, enhancing its reliability when applied to the test dataset.

We chose to split our dataset into folds based on groups of ice shelves. We divided our 128 glaciers

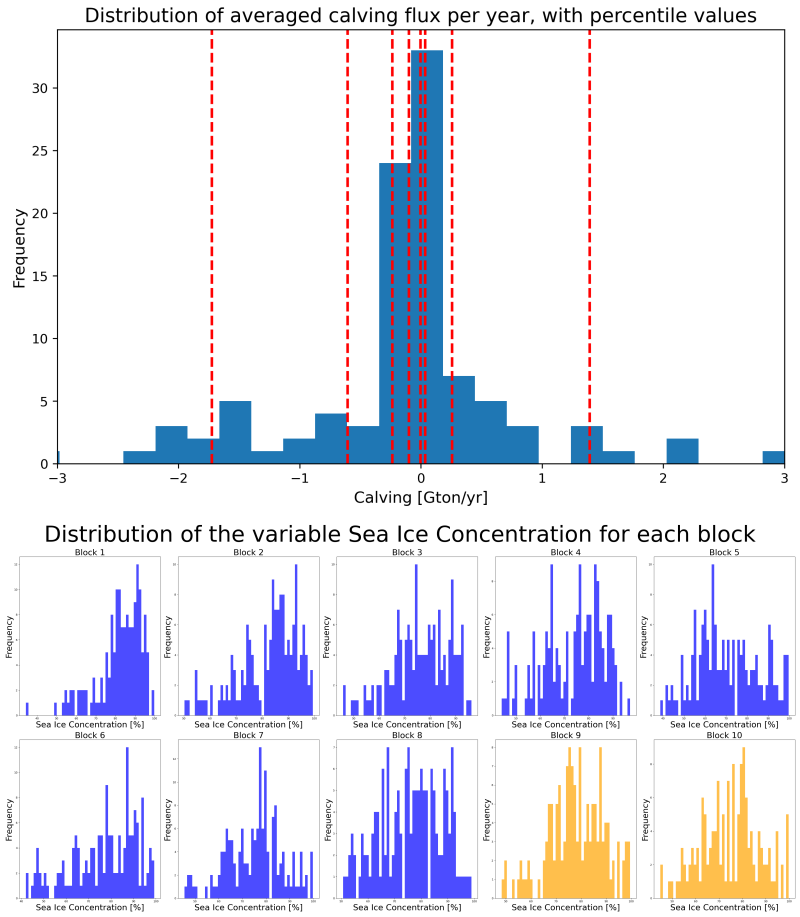

Figure 15: In the upper panel is reported Ice shelf distribution of ice calving averaged per year, with the percentiles reported as red lines. On the lower the Sea Ice concentration distribution across the 10 blocks, in yellow the test block.

into 10 blocks, isolating 2 of them for the test dataset and using the remaining 8 for the training dataset. Each block contains the entire time series of both the target and input features for 12 ice shelves. To divide the ice shelves dataset into the 10 blocks, we followed the block criterion suggested by Robert [41]. Randomly dividing folds might have resulted in the inclusion of spatially dependent (i.e., correlated) data in a block, violating the assumption of dataset independence. This could potentially lead to overfitting of predictions for ice shelves in that region and hinder the generalization to ice shelves from different regions.

As the target variable to predict is calving flux, we adopted a classification approach to categorize

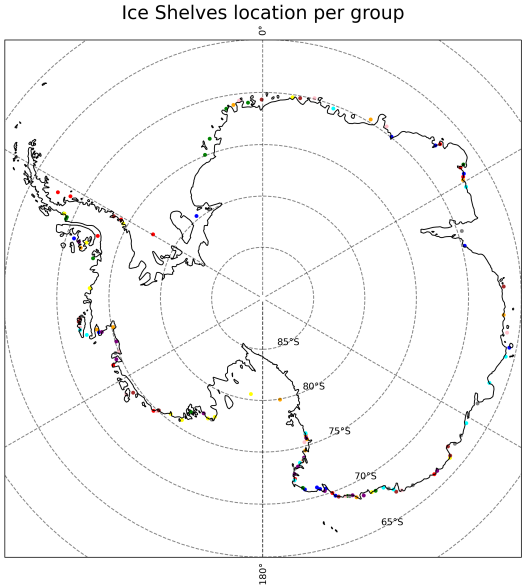

Figure 16: Location of each ice shelf in Antarctica, divided in group by color.

ice shelves based on their average annual calving emissions. This classification ensures balanced representation across different folds in terms of data. Each ice shelf is assigned to one of ten blocks, resulting in each block presenting a representative distribution of average calving emissions per year, maintaining proportional representation across deciles. This classification scheme ensures a balanced distribution of ice shelves exhibiting varying calving rates, thereby enhancing the representativeness of the blocks. While we classified the ice shelves based on their average annual calving emissions, we ensured that the distribution uniformity is respected in the blocks for other variables. Although not as strong as for the calving variable, this uniformity is maintained in the blocks for all other variables, as evident in the lower panel of Figure 15, where the distribution of sea ice concentration per block is depicted. Another check we performed involved examining the geographical distribution of the ice shelves. The left panel of Figure 16 displays the map of the entire Antarctic region, with the location of the ice shelves color-coded by group. As observed, the block division also respects geographical diversity, with glaciers distributed evenly along the continent's coast.

In addition to the dataset partitioning based on the calving classification approach, we employed

random cross-validation as a complementary strategy to establish a baseline for comparison. This random cross-validation allowed us to assess the model's performance under different data splits, providing a reference point for evaluating the effectiveness of our partitioning strategy.

2.6.2 Setting the Hyperparameters: performing the grid search

In the context of machine learning, hyperparameters are external configuration settings that influence the learning process of a model [42]. They are distinct from model parameters, which are learned from the data, and they are set by the modeler as part of the model's architecture. The hyperparameters that we explored in the Random Forest algorithm are as follows:

- **n_estimators**: The number of trees used in the model. Although increasing the number of trees generally improves the performance of the model, it also increases computational time.
- **max_depth**: The maximum depth of each tree in the forest, controlling the maximum number of levels in each decision tree. A deeper tree may capture more complex patterns but could lead to overfitting, while a shorter one could lead to underfitting.
- **min_samples_split**: The minimum number of samples required to split an internal node, controlling how finely the tree is allowed to split the data. A smaller value might lead to overfitting.
- **min_samples_leaf**: The minimum number of samples required to be at a leaf node, controlling the size of the leaves in the tree. Smaller values may lead to overfitting.
- **max_feature**: The number of features to consider when looking for the best split; it controls the randomness of each tree. A smaller value can reduce overfitting.

We decided to explore the potentiality offered by hyperparameter tuning by performing a grid search: a grid search is a research of the hyperparameters values which perform better on the model, according to a specific metric chosen to evaluate it. Providing a set of model hyperparameter ranges, it performs different runs with all the possible hyperparameters combinations, evaluating every time the model according to a provided metric, and identifying therefore the ones

for which the model performed best. We conducted multiple iterations of grid search optimization, initially with a broad exploration of hyperparameter space, encompassing a wide range of values. Subsequently, in the successive iterations this exploration was refined by constraining the hyperparameter ranges, aiming to progressively converge to the optimal combination. The metric we adopted is the Mean Squared Error (MSE).

3 Results and discussion

In this section we will present the results and discuss them. In subsection 3.1 we analyse the input feature trends for the case study of Pine Island, in 3.2 we compare some of the values obtained from our dataset with other present in literature, and finally in 3.3 we analyse the output obtained with our model.

3.1 Input features trends

After completing the tabular dataset, it is now possible to analyze the trends of each variable for each ice shelf. Figure 17 presents an example in the case of Pine Island ice shelf, with the correlation matrix displayed in the lower right panel. In the following paragraphs, we will describe these trends and provide potential interpretations.

The basal melting trend shows a period of relative stability between 2000 and 2010, where the values oscillate between 90 $\frac{Gt}{yr}$ and 110 $\frac{Gt}{yr}$. It then experiences a strong and rapid decrease after 2010, dropping by around 40%, from approximately 100 $\frac{Gt}{yr}$ to 60 $\frac{Gt}{yr}$ in just two years. This is in relatively good agreement with field measurements by Dutrieux's work, which observed a decrease in melting rates of 38% between 2009 and 2012 [43]. This decrease in basal melting rates in 2012 has been attributed to a strong La Niña event.

From the calving time series, three significant calving events can be identified, representing a mass loss greater than 200 $\frac{Gt}{yr}$ in 2001, 2009, and 2014. Other years show relatively small negative values, indicating that the ice shelf did not discharge ice but gained it by re-advancing.

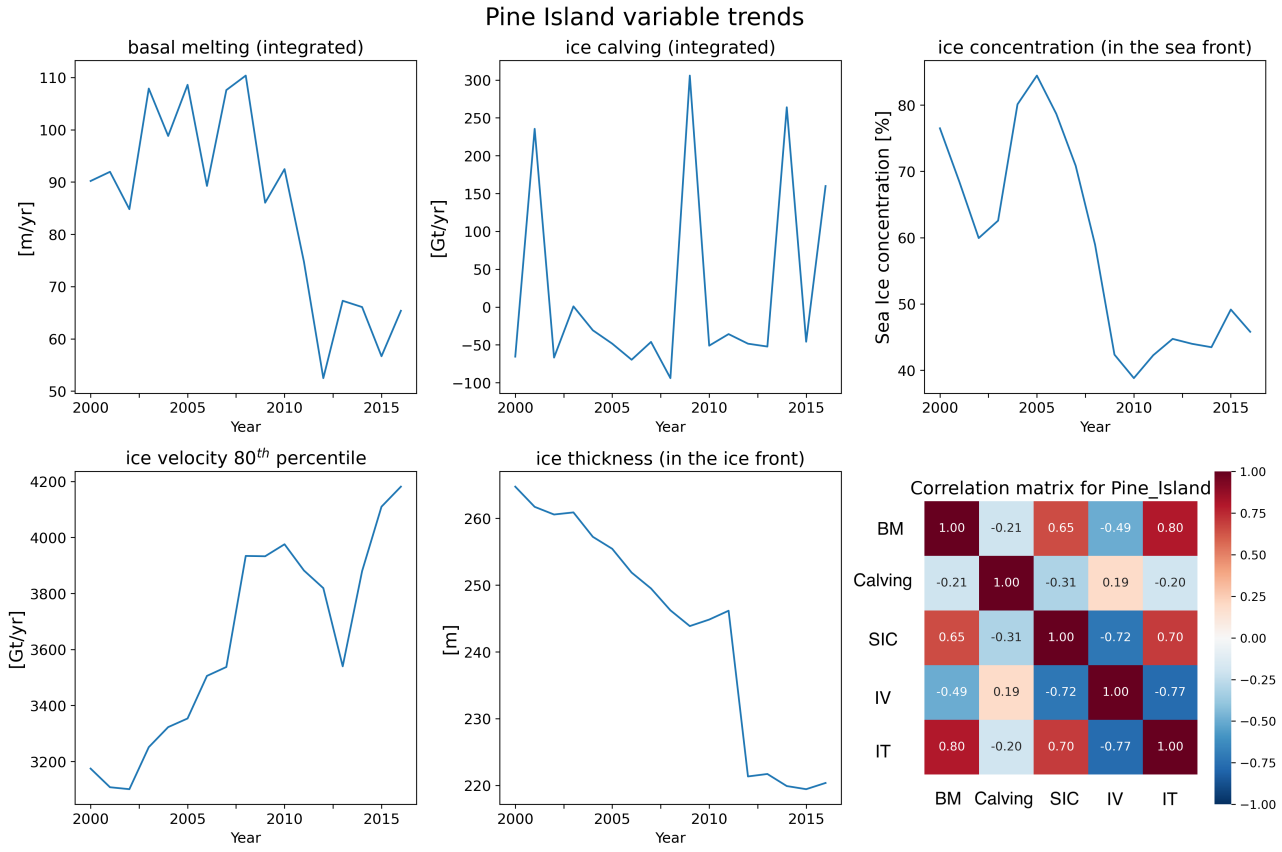

Figure 17: Time series trends for Pine Island ice shelf and correlation matrix. In the correlation matrix BM stands for basal melting, SIC for sea ice concentration, IV for ice velociity and IT for ice thickness. Compared to the other ice shelves, the ones in the Amundsen bay present data from 2000, since it was possible to retrieve velocity data from [23].

The sea ice concentration trend exhibits an oscillatory pattern between 80% and 60% from 2000 to 2005, followed by another drastic decrease, dropping to a minimum of around 40% in 2010. In the last five years, the trend has shown a moderate increase.

The 80^{th} average percentile of ice flow velocity shows a constant increase from 2001 to 2010, when it reaches a first peak of around 3950 $\frac{m}{yr}$. It then slows down till a local minimum of around 3500 $\frac{m}{yr}$ in 2013, followed by a rapid growth until 2017, almost reaching a value of 4200 $\frac{m}{yr}$ in that year.

Ice thickness exhibits an almost constant decrease over the entire analyzed period. From 2000

to 2011, the decrease is not very steep, dropping from around 265m to 245m in 2011. Then, an abrupt fall occurs, reaching approximately 220m in just one year, remaining almost constant for the final period of the analyzed data. Over the entire study period, the ice shelf thinned by almost 50 meters, or 17% of the ice shelf thickness in 2000, with an average ice front thinning rate of 3 m/yr.

The diverse trends depicted here highlight the high level of complexity driving ice shelf changes. Thinning persisted throughout the study period, while basal melting rates decreased, exhibiting a correlation of 0.8 between the two variables. This suggests that a substantial portion of the thinning rate at the calving front may be attributed to dynamic thinning induced by a significant increase in surface flow velocity. This trend is further evidenced by a strong negative correlation of -0.77 between these two variables. The elevated basal melting rates observed from 2000 to 2010 align with the most substantial increase in surface flow velocity over the study period. Spatial-temporal analysis of basal melting rates, as illustrated in Figure 8, indicates that the highest melt rates are concentrated at the grounding line of Pine Island. The grounding line, with its high buttressing potential [44], significantly influences surface flow velocity. This finding aligns with Dutrieux's work, which documented a 20% increase in basal melting rates between 1994 and 2009 [43]. It is noteworthy that the surge in speed followed a large calving event in 2000, suggesting that a reduction in buttressing induced by such an event could impact ice shelf buttressing and increase ice flow velocity. Within the same timeframe, we observed notable changes in sea ice conditions at the Pine Island front, particularly after 2005, when sea ice coverage decreased by approximately 50%. Changes in sea ice conditions have been highlighted as a potentially influential factor in stabilizing glacier/ice shelf fronts, mitigating the impact of destructive ocean swell that can lead to damage and large calving events [45]. After 2010, the frequency of calving events nearly doubled compared to the pre-2010 period. This increase may be attributed to the continued rise in surface flow velocity during this timeframe, which facilitated damage, throughout changes in strain rates, especially in the shear margins [46]. Ice shelf damage has been proposed as a variable closely linked to calving, where fractures and dislocations contribute to a higher number of iceberg

removals from the front [7].

3.2 Comparing results with literature

To validate the datasets employed in our model, we conducted a comparison with results from existing literature. The findings are presented in the following paragraphs.

- Ice-shelf Melting Around Antarctica, Rignot et al 2013 [4]:

  The study conducted by Rignot et al in 2013 provides the initial estimation of basal melting and ice calving for each ice shelf in the Antarctic region during the year 2007-2008. To facilitate a comparison with our datasets, specifically the Green et al and Paulo space-integrated datasets, we examined the Rignot dataset and identified the ice shelves common to all datasets.

  The ice calving value obtained from the Green et al dataset equals $C_{Gr} = 1032 \pm 38 \ \frac{Gt}{yr}$, while the one calculated by Rignot, C_{Ri}, is $C_{Ri} = 1081 \pm 127 \ \frac{Gt}{yr}$, indicating compatibility between the two.

  The integrated value of basal melting BM_{Pa} obtained from the Paulo dataset for all ice shelves shared with the Rignot dataset is $BM_{Pa} = 1292 \pm 388 \ \frac{Gt}{yr}$. The basal melting value calculated by Rignot, BM_{Ri}, is $BM_{Ri} = 1310 \pm 418 \ \frac{Gt}{yr}$. In this case as well, the results are compatible, with both falling within each other's σ range.

- Basal Melting, Adusumilli 2020 [47]:

  Another comparison was made with the work by Adusumilli, who estimated the basal melting per year in the period 1994-2017 to be $1250 \pm 50 \ \frac{Gt}{yr}$. Our estimation for the average basal melting per year from the Paulo dataset was $968 \pm 290 \ \frac{Gt}{yr}$, with results compatible also in this case.

3.3 Random Forest Output

3.3.1 Grid Search

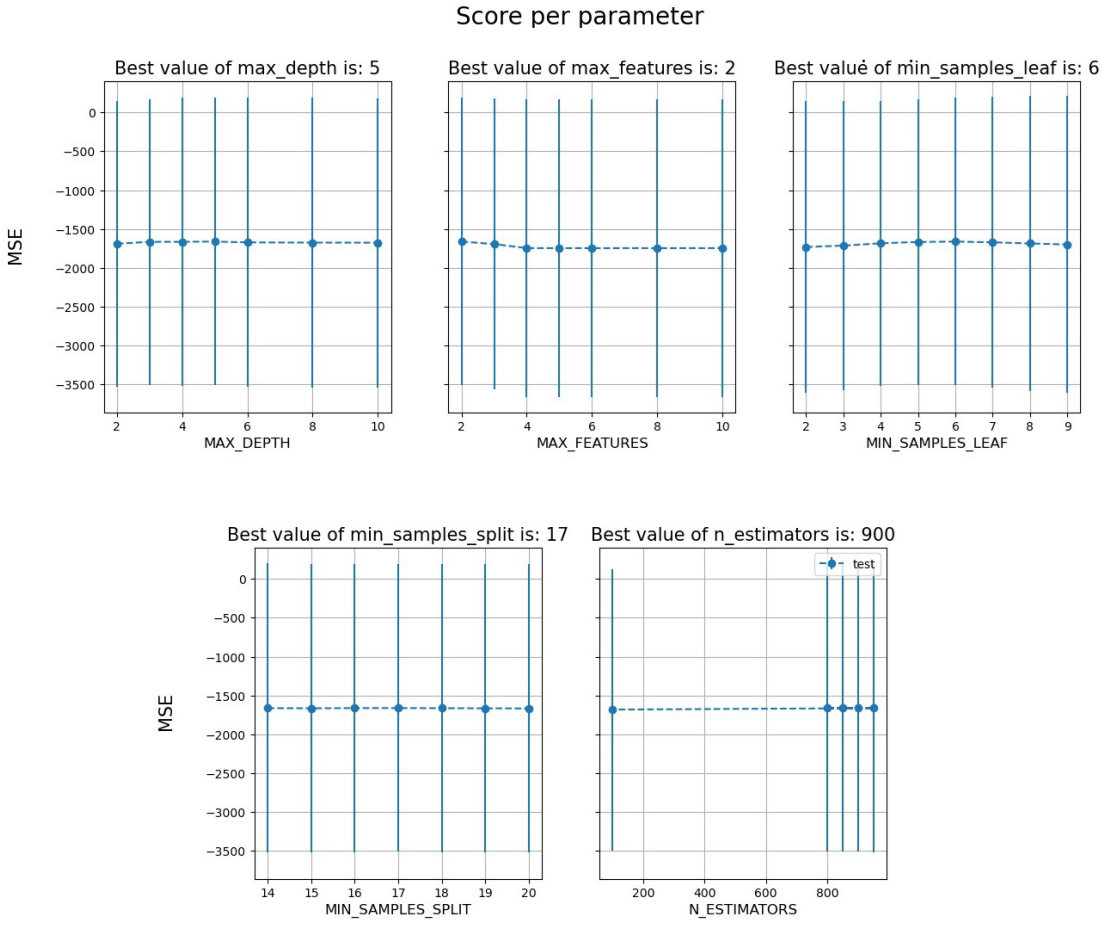

Figure 18: Grid Search Results, where the MSE is reported for each parameter value. The MSEs are obtained by averaging the MSEs obtained by fixing one value of the analysed parameter and running the model with all the possible combination of the other parameters values.

Figure 18 presents the results of the hyperparameter grid search we conducted, depicting Mean Squared Error (MSE) variations with respect to different hyperparameter values. The graphs are generated by fixing one hyperparameter value at a time and running the model multiple times with all possible combinations of the other hyperparameter values. The final MSE is computed by averaging the MSE values obtained in each run with the fixed parameter. This output represents

the culmination of 5 grid searches, each successively narrowing the range of hyperparameters to converge towards the optimal values, which are reported in Table 1.

Max depth	**Max Feature**	**Min sample Leaf**	**Min sample split**	**Number of estimator**
5	2	6	17	900

Table 1: Best results of the hyperparameter grid search

From the output of the grid search, preliminary considerations can be drawn about the final model, which will be built based on these values. The low values for max depth and max features prevent the trees from growing too large and making many splits per node, which helps avoid overfitting but may limit the ability of individual decision trees to comprehend complex behaviors. Regarding the values obtained for min sample leaf and min sample split, the former avoids capturing fine-grained patterns by requiring coarser leaves (a minimum of 6 values), while the latter prevents node creation if there are fewer than 17 values, restricting the extension of the trees. The high values obtained for the number of estimators, which represents the number of decision trees in the forest, suggest that our model has the potential to understand complex dynamics by averaging the decisions of many simple trees.

3.3.2 Model output

We therefore set the model with the best hyperparameters, trained it on the whole train dataset and performed a model run on the test set. From figure 19, where the model calving outputs are plotted against the calving observation, it is possible to make some consideration about the model performance. The degree to which data points converge with the diagonal line signifies the model's proficiency in accurately predicting outcomes, with closer alignment indicating higher predictive accuracy. As it is possible to observe from the graph, the scatterplot shape does not lay along the diagonal, but presents almost an horizontal trend. To have quantitative measures of the model performance we calculated the Root Mean Squared Error (RMSE), the Mean Absolute

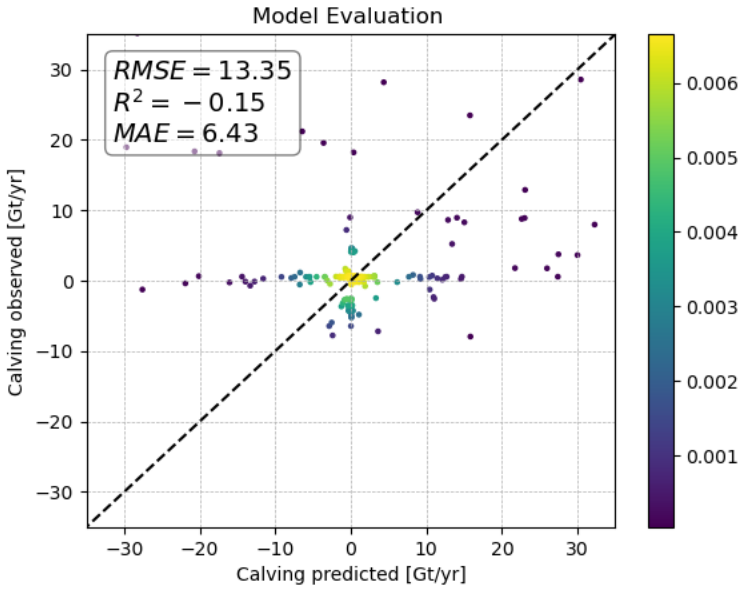

Figure 19: Model simulations vs observations, with the colorbar indicating the point density.

Error (MAE) and the R^2 value, parameters which quantify model accuracy [1]. The latter reveals the proportion of variance in the dependent variable that the model accounts for; a value close to 1 indicates a good fit, value near 0 indicates that the average has the same effectiveness of the model in predicting the output, while a negative value indicates the fact that the mean is better than the model in making predictions. The obtained -0.15 R^2 is indicating the fact that our model predictions are performing worst than the average, and therefore it is failing completely to make accurate predictions. Also, the obtained MAE of 6.5 $\frac{Gt}{yr}$ indicates that on average the calving value predicted by the model is differing of 6.5 $\frac{Gt}{yr}$ compared to the observed value which, considering the fact that for many glacier a calving event rarely surpasses the 10 $\frac{Gt}{yr}$, is quite high. The RMSE value of 13.35 $\frac{Gt}{yr}$ also underscores the model's challenges in accurately predicting calving values. A lower RMSE would signify better performance, but this relatively high value aligns with the limitations highlighted by our analysis, emphasizing the model's difficulty in capturing observed calving variability. From all these observation we can conclude that, despite the steps taken to complete the dataset, the decision to focus just on the region closely involved in the calving events

[1] If $\hat{y}_i$ is the predicted value of the i-th sample and y_i is the corresponding true value for total n samples, the estimated R^2 is defined as: $R^2(y, \hat{y}) = 1 - \frac{\sum_{i=1}^{n}(y_i - \hat{y}_i)^2}{\sum_{i=1}^{n}(y_i - \bar{y})^2}$ where $\bar{y} = \frac{1}{n}\sum_{i=1}^{n} y_i$

and the grid search the model does not succeed in predicting ice calving.

We attribute the primary reason for the under-performance of our model to the utilization of ice-shelf-wide data. As elucidated in the introduction section, spatial information plays a pivotal role in capturing processes occurring in distinct parts of the ice shelf that are intricately interconnected. Phenomena such as ice flow acceleration at the grounding line, ice thinning, and increased basal melting at the ice shelf front are prime examples of interconnected processes that prove challenging to capture through a regional spatial average. These phenomena are, however, crucial in determining the evolution of the ice shelf.

Spatially distributed datasets should be used to try to make ice calving predictions and analysis. These spatially distributed datasets have already been processed in the first part of the internship, and are readily available to be used for training. This opens the door to using Convolutional Neural Networks, capable of exploiting spatial information in the dataset. Due to the limited time available for this project, it was not possible to use them so far. The transition towards this more complex models and richer dataset will be the main focus of the next steps of this study.

3.3.3 Feature Importance

One powerful tool provided by the Random Forest implementation is the analysis of feature importance. As previously mentioned, the Random Forest model determines dataset splits based on the variable that minimizes the Mean Squared Error (MSE) of the target variable in the resulting subsets. The algorithm evaluates how each feature contributes to the decision-making process at each branch, and by averaging across all the trees, it quantifies the importance of each feature. Despite the model's suboptimal performance, analyzing feature importance still offers valuable insights. It is essential to note that interpreting feature importance provides insights into the model's key predictors but does not establish causality. Moreover, these insights are specific to the context of our particular model, considering all its limitations.

According to the feature importance analysis, the two most influential variables affecting ice calving predictions in our model are ice velocity, accounting for approximately 52%, and basal melting

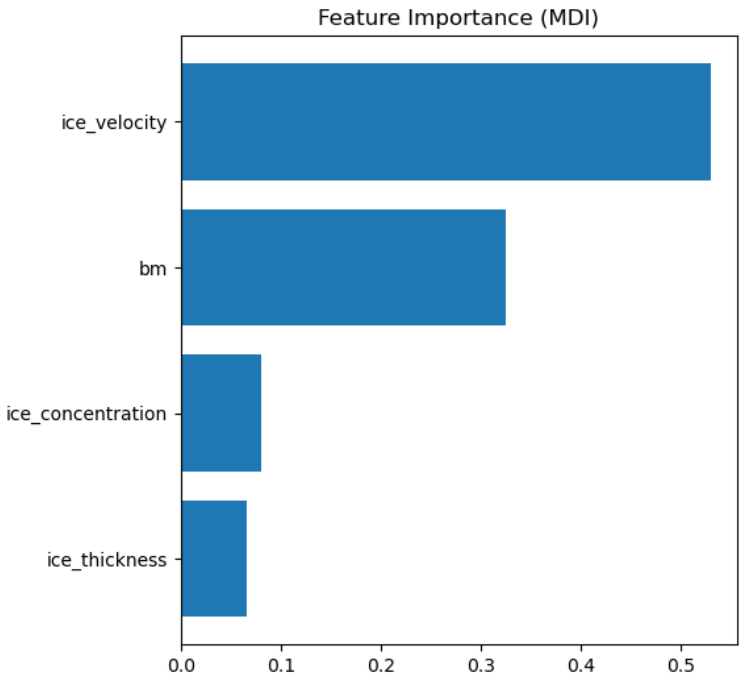

Figure 20: Histogram reporting the importance of the different input features for predicting calving.

(bm), which contributes around 33% to the splits. Ice concentration and ice thickness have less influence on the model's predictions, accounting for approximately 8% and 7%, respectively.

It is interesting to note that the obtained results align with our expectations. Ice velocity and basal melting play a significant role in predicting ice calving events, as the former contributes to crevasse formation due to stress on the ice, and the latter weakens the ice shelf structure, increasing the likelihood of calving events. We expected ice thickness to be quite relevant, given its crucial role in assessing overall ice shelf stability. Different thicknesses also influence thermal and mechanical properties, impacting how the ice shelf responds to external forces such as oceanic and atmospheric conditions. While the precise role of sea ice concentration in buttressing the ice shelf remains uncertain, its importance is acknowledged within the scientific community.

Nonetheless, it is important to interpret these results with caution, particularly due to the low skill of the model in reproducing the observed calving rates.

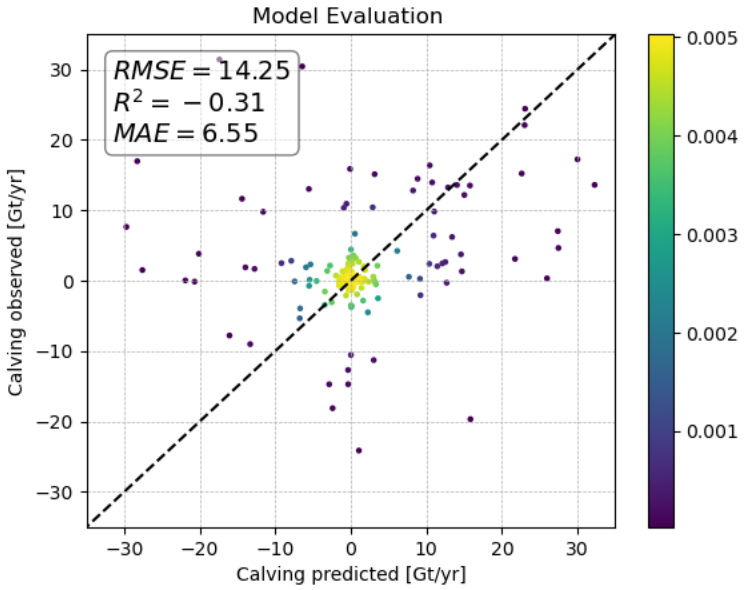

Figure 21: Model simulations vs. observations, with the colorbar indicating the point density. This model was cross-validated with a random split of the test data inside the folds.

3.3.4 Comparing results with the random cross-validation strategy

We employed random cross-validation as a complementary strategy to establish a baseline for comparison with the model output. In this approach, each fold consists of randomly selected values from the dataset, thus not adhering to the inherent spatio-temporal structures present in the data. This randomness in fold creation allows us to assess the model's performance under a scenario that does not consider specific spatial or temporal patterns. It is noteworthy to emphasize that the test set used is the same as the one for the randomly cross-validated model; otherwise, any meaningful comparison would not be possible.

Max depth	Max Feature	Min sample Leaf	Min sample split	Number of estimator
28	2	2	2	36

Table 2: Best results of the hyperparameter grid search for the random cross validated model

To conduct this analysis, we followed the same procedures as those applied to the Random Forest Model, which we utilized with a cross-validation by block strategy. This involved multiple an grid

searches to identify the optimal hyperparameters (with last grid search results reported in Table 2), configuring the model accordingly, and evaluating its performance on the test set.

The scatterplot exhibits an almost horizontal trend, indicating that also in this case the model is not able to make accurate predictions. Examining the quantitative evaluation parameters, we observe that all metrics perform slightly worse than those obtained through block strategy cross-validation, with MAE = $6.55\frac{Gt}{yr}$, RMSE = $14.25\frac{Gt}{yr}$, and R^2 = -0.31 (compared to MAE = $6.43\frac{Gt}{yr}$, RMSE = $13.35\frac{Gt}{yr}$, and R^2 = -0.15).

However, due to the general underperformance of both models and the similarity in evaluation parameters, it is challenging to assess if the block cross-validation strategy resulted in better performance compared to the random one, and it is not possible to conclusively determine which one is superior. These results should be interpreted with caution.

4 Perspectives

In our pursuit of predicting ice calving in Antarctica, we developed a comprehensive spatiotemporal dataset (i.e. a data cube), capturing spatial and temporal information with meticulous standardization. In order to tackle machine learning modelling problems of increasing difficulty, we first decided to use tree-based methods applied to tabular data. For that, we transformed the data cube dataset into a tabular dataset by integrating all spatial distributed information for a single point per ice shelf and year. While this dataset was simpler and it enabled the development of a full machine learning training pipeline, the results were not satisfactory and the model was not capable of learning from the dataset. We argue that the main reasons behind this may lay on the large amount of data compression done when transitioning from the data cube dataset to the tabular one. Consequently, the tabular data was so small that the Random Forest model was not capable of learning the complex nonlinear dynamics from it. Moreover, the spatial distribution of calving rates also carry a lot of information on the physical processes involved in it, and collapsing all distributed data points into a single one per ice shelf might also result in a loss of physical details in the dataset.

Therefore, these first results based on a Random Forest model trained on tabular data hint us to the need of using a more complex machine learning model, namely a U-Net, one of the most used CNNs [48]. The U-Net's proficiency in semantic segmentation, capacity to capture intricate spatial relationships, and adaptability to multimodal datasets make it a strategic choice to address the limitations of the Random Forest model. The phased implementation of the U-Net will involve systematic tuning, adjusting hyperparameters like the learning rate, activation functions, and dropout rates. Hyperparameter optimization techniques, such as grid or random search, will be employed to refine the model's architecture, balancing complexity and generalization, similarly to what has been done for Random Forest. The data cube's distributed representation of ice shelf changes remains crucial for U-Net training, serving as a valuable asset despite time constraints limiting immediate implementation. The optimization and training of the U-Net represent critical steps in unraveling the complexities of Antarctic ice calving, providing a nuanced understanding of the processes involved. We will based our initial architecture choice on previous studies using a U-Net for different problems involving similar datasets in Antarctica (namely the UMelt model from de Roda Husman et al. (in review)).

5 Conclusions

Ice calving remains a poorly understood physical process in ice shelves, contributing to increased uncertainties in predicting the future evolution of ice sheets, particularly in Antarctica. Current attempts to parameterize ice calving in models rely on classical physical equation-based methods, which are often parametrized on a case by case basis, and do not properly capture highly non-linear processes such as damage, which is closely linked to calving. In this study, we adopted a data-driven approach, which has not been explored previously for predicting ice calving in Antarctica. Our objective was to assess the potential of machine learning tools to predict complex and highly non-linear phenomena, such as ice calving.

We first gathered, analyzed, and standardized state-of-the-art remote sensing datasets of physical variables involved in ice calving, namely basal melting, ice thickness, ice velocity, and sea ice

concentration. The variables extend over the antarctic ice shelves and cover the time range 2005-2017. Dataset standardization required a significant effort, as the structure of each dataset differed in terms of temporal and spatial resolution, ice shelf geometry, data coverage, and completeness. Consequently, two datasets were constructed: a data cube, which included spatial information on two dimensions and temporal information on the third dimension, and a tabular dataset derived from the cubic one by summarizing spatial features.

Secondly, we used the tabular dataset as input features for a Random Forest model with the goal of predicting the integrated annual ice calving per ice shelf. The model was optimized by tuning its hyperparameters with a grid search. During cross-validation, we employed two different strategies. Firstly, we manually divided the test dataset into folds to maintain a balanced distribution of ice shelves exhibiting varying calving rates. Secondly, we performed a random split of the test dataset into folds. Unfortunately, both models failed in predicting ice calving on the test set, with the manually divided model achieving slightly better predictive results.

The primary reason for this under-performance is likely the substantial information reduction resulting from summarizing the spatial dataset into a tabular one. This led to a loss of critical spatial information necessary to understand ice-sheet dynamics, such as grounding line dynamics and shear margins strain rates. Nevertheless, we believe that the machine learning approach should not be abandoned following this initial attempt. The data cube (i.e. including a distributed representation of ice shelve changes) is readily available for the training of a Convolutional Neural Network. Unfortunately, due to the limited time available for this project, its implementation was not feasible. The potential of machine learning models remains therefore to be fully exploited in Antarctic ice calving prediction, but they could be a valuable tool to unravel the intricate interactions among the different variables involved in the process. Predicting future ice calving is crucial for accurately quantifying sea level rise, and machine learning stands as a complementary force alongside traditional equation-based models, opening new frontiers to address this problem from a different perspective.

References

[1] J. Weertman. "Stability of the Junction of an Ice Sheet and an Ice Shelf". In: *Journal of Glaciology* 13.67 (1974), pp. 3–11. DOI: 10.3189/S0022143000023327.

[2] E. Rignot et al. "Accelerated ice discharge from the Antarctic Peninsula following the collapse of Larsen B ice shelf". In: *Geophysical Research Letters* 31.18 (2004). DOI: https://doi.org/10.1029/2004GL020697.

[3] Sainan Sun et al. "Antarctic ice sheet response to sudden and sustained ice-shelf collapse (ABUMIP)". In: *Journal of Glaciology* 66.260 (2020), pp. 891–904. DOI: 10.1017/jog.2020.67.

[4] E. Rignot et al. "Ice-Shelf Melting Around Antarctica". In: *Science (New York, N.Y.)* 341 (June 2013). DOI: 10.1126/science.1235798.

[5] HD Pritchard et al. "Antarctic ice-sheet loss driven by basal melting of ice shelves". In: *Nature* 484.7395 (Apr. 2012), pp. 502–505. ISSN: 0028-0836. DOI: 10.1038/nature10968. URL: https://doi.org/10.1038/nature10968.

[6] Ted Scambos et al. "Ice shelf disintegration by plate bending and hydro-fracture: Satellite observations and model results of the 2008 Wilkins ice shelf break-ups". In: *Earth and Planetary Science Letters* 280.1 (2009), pp. 51–60. ISSN: 0012-821X. DOI: https://doi.org/10.1016/j.epsl.2008.12.027. URL: https://www.sciencedirect.com/science/article/pii/S0012821X08007887.

[7] Sainan Sun and G. Hilmar Gudmundsson. "The speedup of Pine Island Ice Shelf between 2017 and 2020: revaluating the importance of ice damage". In: *Journal of Glaciology* (2023), pp. 1–9. DOI: 10.1017/jog.2023.76.

[8] Y. Choi et al. "Comparison of four calving laws to model Greenland outlet glaciers". In: *The Cryosphere* 12.12 (2018), pp. 3735–3746. DOI: 10.5194/tc-12-3735-2018. URL: https://tc.copernicus.org/articles/12/3735/2018/.

[9] J. A. Wilner, M. Morlighem, and G. Cheng. "Evaluation of four calving laws for Antarctic ice shelves". In: *The Cryosphere Discussion* (2023), pp. 1–19. DOI: 10.5194/tc-2023-86. URL: https://tc.copernicus.org/preprints/tc-2023-86/.

[10] Douglas I. Benn, Nicholas R.J. Hulton, and Ruth H. Mottram. "'Calving laws', 'sliding laws' and the stability of tidewater glaciers". In: *Annals of Glaciology* 46 (2007), pp. 123–130. DOI: 10.3189/172756407782871161.

[11] M. Morlighem et al. "Modeling the response of northwest Greenland to enhanced ocean thermal forcing and subglacial discharge". In: *The Cryosphere* 13.2 (2019), pp. 723–734. DOI: 10.5194/tc-13-723-2019. URL: https://tc.copernicus.org/articles/13/723/2019/.

[12] A. Levermann et al. "Kinematic first-order calving law implies potential for abrupt ice-shelf retreat". In: *The Cryosphere* 6.2 (2012), pp. 273–286. DOI: 10.5194/tc-6-273-2012. URL: https://tc.copernicus.org/articles/6/273/2012/.

[13] J. Bolibar et al. "Deep learning applied to glacier evolution modelling". In: *The Cryosphere* 14 (2020), pp. 565–584.

[14] Chris Rackauckas et al. "Universal Differential Equations for Scientific Machine Learning". In: (Jan. 2020). DOI: 10.21203/rs.3.rs-55125/v1.

[15] Redouane Lguensat et al. "Learning Generalized Quasi-Geostrophic Models Using Deep Neural Numerical Models". In: (Nov. 2019).

[16] Maziar Raissi, Paris Perdikaris, and George Karniadakis. "Physics Informed Deep Learning (Part I): Data-driven Solutions of Nonlinear Partial Differential Equations". In: (Nov. 2017).

[17] Zewen Li et al. "A Survey of Convolutional Neural Networks: Analysis, Applications, and Prospects". In: *IEEE Transactions on Neural Networks and Learning Systems* PP (June 2021), pp. 1–21. DOI: 10.1109/TNNLS.2021.3084827.

[18] L Breiman. "Random Forests". In: *Machine Learning* 45 (Oct. 2001), pp. 5–32. DOI: 10.1023/A:1010950718922.

[19] F. S. Paolo et al. "Widespread slowdown in thinning rates of West Antarctic ice shelves". In: *The Cryosphere* 17.8 (2023), pp. 3409–3433. DOI: 10.5194/tc-17-3409-2023. URL: https://tc.copernicus.org/articles/17/3409/2023/.

[20] Mathieu Depoorter et al. "Corrigendum: Calving fluxes and basal melt rates of Antarctic ice shelves". In: *Nature* 502 (Sept. 2013). DOI: 10.1038/nature12567.

[21] E. Rignot, J. Mouginot, and B. Scheuchl. *MEaSUREs InSAR-Based Antarctica Ice Velocity Map, Version 2*. 2017. DOI: 10.5067/D7GK8F5J8M8R. URL: https://nsidc.org/data/NSIDC-0484/versions/2.

[22] J. Mouginot, E. Rignot, and B. Scheuchl. *Continent-Wide, Interferometric SAR Phase, Mapping of Antarctic Ice Velocity*. 2019. DOI: https://doi.org/10.1029/2019GL083826. URL: https://agupubs.onlinelibrary.wiley.com/doi/abs/10.1029/2019GL083826.

[23] E. Rignot, J. Mouginot, and B. Scheuchl. *MEaSUREs InSAR-Based Ice Velocity of the Amundsen Sea Embayment, Antarctica, Version 1*. 2014. DOI: 10.5067/MEASURES/CRYOSPHERE/nsidc-0545.001. URL: https://nsidc.org/data/NSIDC-0545/versions/1.

[24] Eric Rignot et al. *Four decades of Antarctic Ice Sheet mass balance from 1979–2017*. Proceedings of the National Academy of Sciences, 2019. DOI: doi:10.1073/pnas.1812883116.

[25] A. Gardner, M. Fahnestock, and T. Scambos. "MEaSUREs ITS_LIVE Regional Glacier and Ice Sheet Surface Velocities, Version 1". In: (2022). DOI: 10.5067/6II6VW8LLWJ7. URL: https://nsidc.org/data/NSIDC-0776/versions/1.

[26] Gardner Greene and Fraser Schlegel. *Antarctic calving loss rivals ice-shelf thinning*. 2022. DOI: 10.1038/s41586-022-05037-w. URL: https://tc.copernicus.org/articles/17/3409/2023/.

[27] W. N. Meier et al. *NOAA/NSIDC Climate Data Record of Passive Microwave Sea Ice Concentration, Version 4*. 2021. DOI: 10.7265/efmz-2t65. URL: https://nsidc.org/data/G02202/versions/4.

[28] D. J. Cavalieri, P. Gloersen, and W. J. Campbell. "Determination of sea ice parameters with the NIMBUS 7 SMMR". In: *Journal of Geophysical Research: Atmospheres* 89 (1984), pp. 5355–5369. DOI: https://doi.org/10.1029/JD089iD04p05355.

[29] J. C. Comiso. "Characteristics of Arctic winter sea ice from satellite multispectral microwave observations". In: *Journal of Geophysical Research: Oceans* 91 (1986), pp. 975–995. DOI: https://doi.org/10.1029/JC091iC01p00975.

[30] M. Morlighem. *MEaSUREs BedMachine Antarctica, Version 3*. 2022. DOI: 10.5067/FPSU0V1MWUB6. URL: https://nsidc.org/data/NSIDC-0756/versions/3.

[31] Hongxing Liu and Kenneth Jezek. "A Complete High-Resolution Coastline of Antarctica Extracted from Orthorectified Radarsat SAR Imagery". In: *Photogrammetric Engineering Remote Sensing* 70 (May 2004), pp. 605–616. DOI: 10.14358/PERS.70.5.605.

[32] A. D. Fraser et al. "High-resolution mapping of circum-Antarctic landfast sea ice distribution, 2000–2018". In: *Earth System Science Data* 12.4 (2020), pp. 2987–2999. DOI: 10.5194/essd-12-2987-2020. URL: https://essd.copernicus.org/articles/12/2987/2020/.

[33] A. Gardner, M. Fahnestock, and T. Scambos. *MEaSUREs ITS_LIVE Regional Glacier and Ice Sheet Surface Velocities, Version 1*. 2022. DOI: 10.5067/6II6VW8LLWJ7. URL: https://nsidc.org/data/NSIDC-0776/versions/1.

[34] M. Morlighem. *MEaSUREs BedMachine Antarctica, Version 2*. 2020. DOI: 10.5067/E1QL9HFQ7A8M. URL: https://nsidc.org/data/NSIDC-0756/versions/2.

[35] E. Rignot, J. Mouginot, and B. Scheuchl. "Antarctic grounding line mapping from differential satellite radar interferometry". In: *Geophysical Research Letters* 38 (2011). DOI: https://doi.org/10.1029/2011GL047109.

[36] E. Rignot et al. "Widespread, rapid grounding line retreat of Pine Island, Thwaites, Smith, and Kohler glaciers, West Antarctica, from 1992 to 2011". In: *Geophysical Research Letters* 41 (2014), pp. 3502–3509. DOI: https://doi.org/10.1002/2014GL060140.

[37] D. E. Shean et al. "Ice shelf basal melt rates from a high-resolution digital elevation model (DEM) record for Pine Island Glacier, Antarctica". In: *The Cryosphere* 13 (2019), pp. 2633–2656. DOI: 10.5194/tc-13-2633-2019.

[38] Pauli Virtanen et al. "SciPy 1.0: Fundamental Algorithms for Scientific Computing in Python". In: *Nature Methods* 17 (2020), pp. 261–272. DOI: 10.1038/s41592-019-0686-2.

[39] Stefan Van der Walt et al. "scikit-image: image processing in Python". In: *PeerJ* 2 (2014), e453.

[40] scikit-learn. *Cross-Validation scheme*. [Online; accessed December 3,2023]. 2010. URL: https://scikit-learn.org/stable/modules/cross_validation.html.

[41] David R. Roberts et al. "Cross-validation strategies for data with temporal, spatial, hierarchical, or phylogenetic structure". In: *Echography* 8 (2017), pp. 913–929. DOI: https://doi.org/10.1111/ecog.02881.

[42] Philipp Probst, Marvin N. Wright, and Anne-Laure Boulesteix. "Hyperparameters and tuning strategies for random forest". In: *WIREs Data Mining and Knowledge Discovery* 9.3 (Jan. 2019). ISSN: 1942-4795. DOI: 10.1002/widm.1301. URL: http://dx.doi.org/10.1002/widm.1301.

[43] Pierre Dutrieux et al. "Strong Sensitivity of Pine Island Ice-Shelf Melting to Climatic Variability". In: *Science* 343 (2014), pp. 174–178. DOI: 10.1126/science.1244341.

[44] Johannes Jakob Fürst et al. "The safety band of Antarctic ice shelves". In: *Nature Climate Change* 6.5 (May 2016), pp. 479–482. DOI: 10.1038/nclimate2912.

[45] Rob Massom et al. "Antarctic ice shelf disintegration triggered by sea ice loss and ocean swell". In: *Nature* 558 (June 2018). DOI: 10.1038/s41586-018-0212-1.

[46] Stef Lhermitte et al. "Damage accelerates ice shelf instability and mass loss in Amundsen Sea Embayment". In: *Proceedings of the National Academy of Sciences of the United States of America* 117 (Sept. 2020). DOI: 10.1073/pnas.1912890117.

[47] Susheel Adusumilli et al. "Interannual variations in meltwater input to the Southern Ocean from Antarctic ice shelves". In: *Nature Geoscience* 13 (Sept. 2020), pp. 1–5. DOI: 10.1038/s41561-020-0616-z.

[48] Olaf Ronneberger, Philipp Fischer, and Thomas Brox. "U-Net: Convolutional Networks for Biomedical Image Segmentation". In: vol. 9351. Oct. 2015, pp. 234–241. ISBN: 978-3-319-24573-7. DOI: 10.1007/978-3-319-24574-4_28.

Code Availability

The code employed for the machine learning aspect of this project is accessible through a dedicated GitHub repository. Currently, this repository is undergoing refinement to enhance clarity, and a comprehensive readme file is being added to improve its shareability.

machine learning part :https://github.com/Moncada-Francesco-97/machine_learning_calving_project

For the preprocessing part, a directory is yet to be established to compile the local and cluster codes used in generating the dataset.